

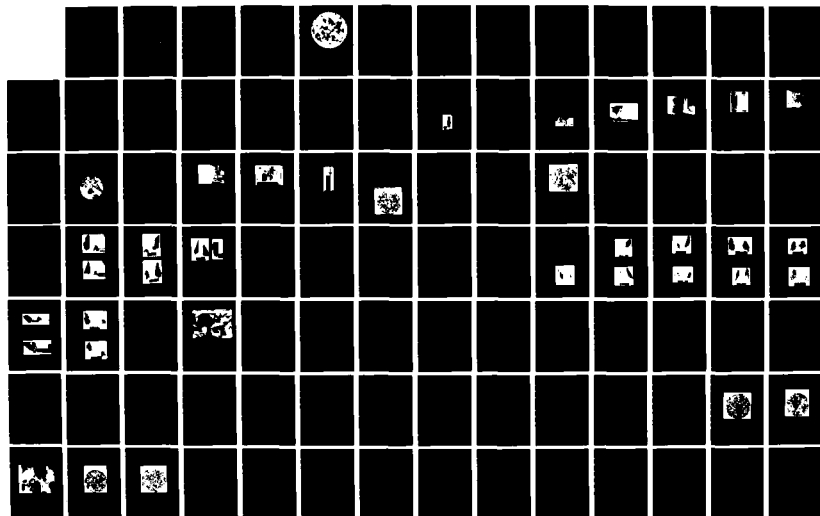
AD-A162 361

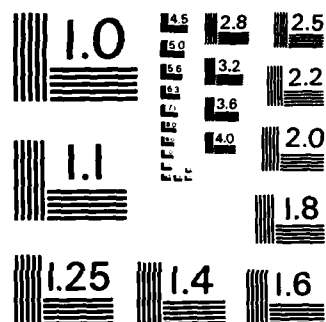
THE EFFECT OF A BIMODAL GRAIN SIZE DISTRIBUTION ON THE
COMPRESSIVE STRENGTH OF POLYCRYSTALLINE ICE(U) ARMY
MILITARY PERSONNEL CENTER ALEXANDRIA VA J L LAUGHLIN
DEC 85 F/G 8/12

1/2

UNCLASSIFIED

NL





MICROCOPY RESOLUTION TEST CHART
NATIONAL BUREAU OF STANDARDS - 1963 - A

AD-A162 361

SECURITY CLASSIFICATION OF THIS PAGE (When Data Entered)

REPORT DOCUMENTATION PAGE		READ INSTRUCTIONS BEFORE COMPLETING FORM
1. REPORT NUMBER	2. GOVT ACCESSION NO. AD-A162 361	3. RECIPIENT'S CATALOG NUMBER
4. TITLE (and Subtitle) The effect of a bimodal grain size distribution on the compressive strength of polycrystalline ice		5. TYPE OF REPORT & PERIOD COVERED Final Report December 1985
7. AUTHOR(s) MAJ James L Laughlin		6. PERFORMING ORG. REPORT NUMBER
9. PERFORMING ORGANIZATION NAME AND ADDRESS Student, HQDA, MILPERCEN (DAPC-OPA-E) 200 Stovall Street, Alexandria, Virginia 22332		8. CONTRACT OR GRANT NUMBER(s)
11. CONTROLLING OFFICE NAME AND ADDRESS HQDA, MILPERCEN, ATTN: DAPC-OPA-E 200 Stoval Street, Alexandria Virginia, 22332		10. PROGRAM ELEMENT, PROJECT, TASK AREA & WORK UNIT NUMBERS
14. MONITORING AGENCY NAME & ADDRESS (if different from Controlling Office)		12. REPORT DATE December 1985
		13. NUMBER OF PAGES
		15. SECURITY CLASS. (of this report)
		15a. DECLASSIFICATION/DOWNGRADING SCHEDULE
16. DISTRIBUTION STATEMENT (of this Report) Approved for public release; distribution unlimited		
17. DISTRIBUTION STATEMENT (of the abstract entered in Block 20, if different from Report) A		
18. SUPPLEMENTARY NOTES Thesis submitted to Thayer School of Engineering, Dartmouth College		
19. KEY WORDS (Continue on reverse side if necessary and identify by block number) Polycrystalline Ice Ih, Compressive strength of ice, Bimodal grain size distribution of polycrystalline ice		
20. ABSTRACT (Continue on reverse side if necessary and identify by block number) Previous studies by Thayer School graduates have shown that the grain size directly affects the strength of fresh-water equiaxed polycrystalline ice Ih, where the strength decreases as the grain size increases. This has been shown both in tension and compression at constant strain rates over a range of temperatures (-5 C, -10 C, -20 C). The mechanical behavior of the ice is well described by the Hall-Petch relation. This work presents the results of a study to examine the effect of a bimodal		

DD FORM 1 JAN 73 1473 EDITION OF 1 NOV 65 IS OBSOLETE

DTIC FILE COPY

SECURITY CLASSIFICATION OF THIS PAGE (When Data Entered)

85 12 16 161

10.00001/s and 0.001/s.

SECURITY CLASSIFICATION OF THIS PAGE(When Data Entered)

grain size distribution on the compressive strength of equiaxed randomly oriented polycrystalline ice Ih. Laboratory prepared specimens of right circular cylindrical ice consisting of different amounts of large (5.5 mm) and small (2.0 mm) grains by volume (75%/25%, 50%/50%, 25%/75%) were tested at -10 C in uniaxial unconfined compression. Tests were conducted at two strain rates, 10^{-5} s^{-1} and 10^{-3} s^{-1} .

Building on the results of Cannon (1985), this work establishes the law of mixtures for the compressive strength of a specimen composed of a bimodal mix of grains. First hypothesized by Lee (1985), the law of mixtures states that the strength of a bimodal specimen is linearly dependent on the volume fraction of large and small grains. A single significant grain size may be used to characterize the mechanical behavior of the specimen. Two possible candidates of a significant grain size are examined, one derived from the use of the Hall-Petch relation and the second being the average of the two grain sizes. Results show the use of the average is more expedient with little loss in accuracy.

This work also investigates the strength of unimodal polycrystalline ice tested in compression at a strain rate of 10^{-1} s^{-1} , $t = -10 \text{ C}$. Consistent with finding of others, Cole, (1985), the compressive strength decreases with increasing grain size.

SECURITY CLASSIFICATION OF THIS PAGE(When Data Entered)

The effect of a bimodal grain size distribution on the compressive strength of polycrystalline ice.

James L Laughlin, MAJ
HQDA, MILPERCEN (DAPC-OPA-E)
200 Stovall Street
Alexandria, Virginia 22332

Final Report December 1985

Approved for public release; distribution unlimited



Accession For	
1	<input checked="" type="checkbox"/>
2	<input type="checkbox"/>
3	<input type="checkbox"/>
4	<input type="checkbox"/>
5	<input type="checkbox"/>
6	<input type="checkbox"/>
7	<input type="checkbox"/>
8	<input type="checkbox"/>
9	<input type="checkbox"/>
10	<input type="checkbox"/>
Dist	
A1	

A thesis submitted to Thayer School of Engineering, Dartmouth College
in partial fulfillment of the requirements for the degree of Master of Engineering



Ice Research Laboratory

Thayer School of Engineering • Dartmouth College
Hanover, New Hampshire 03755

The Effect of a Biomodal Grain Size Distribution on the
Compressive Strength of Polycrystalline Ice

A Thesis

Submitted to the Faculty
in partial fulfillment of the requirements for the
degree of
Master of Engineering

by

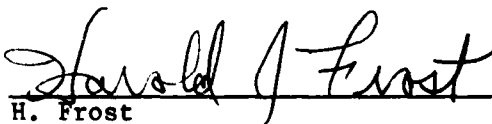
James L. Laughlin


Thayer School of Engineering
Dartmouth College
Hanover, NH 03755

December, 1985

Examining Committee:


E. Schulson - Chairman


H. Frost


W. Nixon


Dean, Thayer School of Engineering


Signature of Author

Thayer School of Engineering
Dartmouth College

The Effect of a Bimodal Grain Size Distribution on the
Compressive Strength of Polycrystalline Ice

James L. Laughlin

Master of Engineering
December, 1985

ABSTRACT

This work presents the results of a study to examine the effect of a bimodal grain size distribution on the compressive strength of equiaxed randomly oriented polycrystalline ice Ih. Laboratory prepared specimens of right circular cylindrical ice consisting of different amounts of large (5.5 mm) and small (2.0 mm) grains by volume (75%/25%, 50%/50%, 25%/75%) were tested at -10°C in uniaxial unconfined compression. Tests were conducted at two strain rates, 10^{-5}s^{-1} and 10^{-3}s^{-1} .

Building on the results of Cannon (1985), this work establishes the law of mixtures for the compressive strength of a specimen comprised of a bimodal mix of grains, first hypothesized by Lee (1985). The strength of the bimodal specimen in (MPa) is:

$$\sigma_{\text{bimodal}} = f_L \sigma_L + f_S \sigma_S$$

where, f_L = fraction large grain, f_S = fraction small grain and σ_L and σ_S are strengths of large and small grain unimodal specimens respectively. A single significant grain size may be used to compute the compressive strength of the specimen. Two possible candidates of significant grain size are examined.

This work also investigates the strength of polycrystalline ice of a unimodal distribution, tested in compression at a strain rate of 10^{-1}s^{-1} , $T = -10^{\circ}\text{C}$. Consistent with findings at other strain rates (Cannon (1985) and Cole (1985)), the compressive strength decreases with increasing grain size.

Acknowledgements

I wish to thank my thesis committee for their patience and assistance in the completion of my studies. I am especially grateful to Professor Schulson who was willing to spend much time in teaching me many fine points needed to complete my research.

Many thanks to Russ Lee for his sense of humor and for shining the light through the darkness. I would also like to thank Prof Wilf Nixon for his willing help and expertise.

Without the folks at CRREL there would have been no project at all. Steve Ackley, Tony Gow, Nancy Perron and Glenn Durrell were all instrumental in the beginning. Thanks are also due to Debbie Call for her efforts in producing this manuscript.

I am indebted to the U.S Army for funding my education and the Ice Research Center, Dartmouth College for allowing me to use the facilities for my experimentation.

Finally, allow me to thank my wife for her understanding during the many hours when things were not going well and for preventing my head from swelling when they were. Without her and my family, this achievement would have far less meaning.

TABLE OF CONTENTS

	<u>Page</u>
ABSTRACT	ii
ACKNOWLEDGEMENTS	iii
TABLE OF CONTENTS	iv
LIST OF TABLES	vi
LIST OF FIGURES	vii
1. INTRODUCTION	1
2. BACKGROUND	3
2.1 Grain Size Dependence	3
2.2 Law of Mixtures	5
3. PROCEDURE	7
3.1 General Technique	7
3.1.1 Equipment Used	8
3.1.2 Water Preparation	8
3.1.3 Seed Grains	10
3.1.4 Sample Preparation	12
3.1.5 Bimodal Samples	15
3.2 Testing Procedures	17
3.3 Post-test Procedures	21
3.4 Sample Quality	22
4. RESULTS	23
4.1 Bimodal Tests at 10^{-5} s^{-1}	23
4.2 Bimodal Tests at 10^{-3} s^{-1}	28
4.3 Strain at Peak or Fracture Stress	35
4.4 Unimodal Tests at 10^{-1} s^{-1}	36
5. ANALYSIS AND DISCUSSION	45
5.1 Cracking Activity	45
5.2 Law of Mixtures	46
5.3 Significant Grain Size	50
5.4 Unimodal Tests at 10^{-1} s^{-1}	57
6. CONCLUSIONS	64

	<u>Page</u>
7. SUGGESTIONS FOR FUTURE RESEARCH	66
8. REFERENCES	67
APPENDIX A	69
APPENDIX B	74
APPENDIX C	92

LIST OF TABLES

<u>Table #</u>	<u>Caption</u>	<u>Page</u>
4.1	Comparison of Desired vs. Actual Grain Distribution	25
4.2	Cracking Activity at a Strain Rate of 10^{-5} s^{-1} , $T = -10^{\circ}\text{C}$	26
4.3	Results at a Strain Rate of 10^{-5} s^{-1} , $T = -10^{\circ}\text{C}$	27
4.4	Samples Pictured in Figure 4.5	29
4.5	Results at a Strain Rate of 10^{-3} s^{-1} , $T = -10^{\circ}\text{C}$	33
4.6	Unimodal Results at a Strain Rate of 10^{-1} s^{-1} , $T = -10^{\circ}\text{C}$	37
5.1	Comparison of Projected Strength to Actual Strength with $d_{\text{sig}} = d_{\text{HP}}$ at a Strain Rate of 10^{-5} s^{-1} , $T = -10^{\circ}\text{C}$	52
5.2	Comparison of Projected Strength to Actual Strength with $d_{\text{sig}} = d_{\text{HP}}$ at a Strain Rate of 10^{-3} s^{-1} , $T = -10^{\circ}\text{C}$	54
5.3	Comparison of Predicted Strength for $d_{\text{sig}} = d_{\text{HP}}$ and $d_{\text{sig}} = d_{\text{avg}}$ to Actual Strength at a Strain Rate of 10^{-5} s^{-1} , $T = -10^{\circ}\text{C}$	54
5.4	Sample Number and Grain Size Mix	55
5.5	Comparison of Predicted Strength for $d_{\text{sig}} = d_{\text{HP}}$ and $d_{\text{sig}} = d_{\text{avg}}$ to Actual Strength at a Strain Rate of 10^{-5} s^{-1} , $T = -10^{\circ}\text{C}$	56
5.6	Comparison of Predicted Strength for $d_{\text{sig}} = d_{\text{HP}}$ and $d_{\text{sig}} = d_{\text{avg}}$ to Actual Strength at a Strain Rate of 10^{-3} s^{-1} , $T = -10^{\circ}\text{C}$	56
C.1	Stroke Control Results at Strain Rate of 10^{-1} s^{-1} , $T = -10^{\circ}\text{C}$	92

LIST OF FIGURES

<u>Figure #</u>	<u>Caption</u>	<u>Page</u>
3.1	Photograph of Molding Apparatus	8
3.2	Schematic of Molding Apparatus	9
3.3	Water Preparation Equipment	10
3.4	Ice Sheets and Pans	11
3.5	Sieves and Seed Grains	12
3.6	Prepared Samples after Removal from Mold	13
3.7	Mold in Freezing Apparatus Connected to Water Tank and Vacuum Pump	14
3.8	Photograph of Thin Section (Lee (1985)) Showing Bimodal Sample after Testing at Strain Rate of 10^{-6} s^{-1} , $T = -10^{\circ}\text{C}$	16
3.9	Photograph of CRREL MTS	18
3.10	Photograph of IRL MTS During Testing, $T = -10^{\circ}\text{C}$	19
3.11	Photograph of Sample Quality Check on Comparator	20
3.12	Photograph of Thin Section after Testing at Strain Rate of 10^{-5} s^{-1} , $T = -10^{\circ}\text{C}$	21
4.1	Photograph of Thin Section after Testing at Strain Rate of 10^{-5} s^{-1} , $T = -10^{\circ}\text{C}$	24
4.2	Peak Stress vs. Volume Fraction of Large Grains for Strain Rate of 10^{-5} s^{-1} , $T = -10^{\circ}\text{C}$	28
4.3	Photograph of Samples after Test at a Strain Rate of 10^{-3} s^{-1} , $T = -10^{\circ}\text{C}$	30
4.4	Fracture Stress vs. Volume Fraction of Large Grains for Strain Rate of 10^{-3} s^{-1} , $T = -10^{\circ}\text{C}$	34
4.5	Strain at Peak or Fracture Stress vs. Volume Fraction of Large Grains, $T = -10^{\circ}\text{C}$	36

<u>Figure #</u>	<u>Caption</u>	<u>Page</u>
4.6	Fracture Stress vs. Grain Size for a Strain Rate of 10^{-1}s^{-1} , $T = -10^{\circ}\text{C}$	37
4.7	Photographs of Samples Tested at Strain Rate of 10^{-1}s^{-1} , $T = -10^{\circ}\text{C}$	38
5.1	Photograph of a Magnified View (7X) of a Thin Section from Specimen Tested at Strain Rate of 10^{-5}s^{-1} , $T = -10^{\circ}\text{C}$	46
5.2	Peak Stress vs. Volume Fraction of Large Grains for Strain Rate of 10^{-5}s^{-1} , $T = -10^{\circ}\text{C}$, with Plot of Predicted Strength from Law of Mixtures	47
5.3	Fracture Stress vs. Volume Fraction of Large Grains for Strain Rate of 10^{-5}s^{-1} , $T = -10^{\circ}\text{C}$ with Plot of Predicted Strength from Law of Mixtures	49
5.4	Standard Deviation of Peak Stress at Strain Rate of 10^{-3}s^{-1} vs. Volume Fraction of Large Grain, $T = -10^{\circ}\text{C}$	50
5.5	Fracture Stress at a Strain Rate of 10^{-3}s^{-1} vs. the Inverse Square Root of the Grain Size, $T = -10^{\circ}\text{C}$	53
5.6	Stress vs. the Inverse Square Root of the Grain Size, $T = -10^{\circ}\text{C}$	58
5.7	Stress vs. Strain on a Log-Log Plot for $d = 3.8 \pm .4 \text{ mm}$	61
5.8	Stress vs. Strain on a Log-Log Plot for $d = 5.5 \pm .5 \text{ mm}$	62
5.9	Stress vs. Strain on a Log-Log Plot for $d = 7.0 \pm .7 \text{ mm}$	63
A.1-5	Thin Section Photographs of Samples Tested at Strain Rate of 10^{-5}s^{-1} , $T = -10^{\circ}\text{C}$	69
B.1	Stress Strain Curves for Samples Tested at Strain Rate of 10^{-5}s^{-1} and 10^{-3}s^{-1} , $T = -10^{\circ}\text{C}$	74
C.1	Peak Stress in Stroke Control vs. Grain Size, $T = -10^{\circ}\text{C}$	93

1. INTRODUCTION

There have been a number of studies (Currier (1981), Lim (1983), and Lee (1985)) that have clearly shown the inverse relationship that exists between the strength of ice in tension and the grain size found in the polycrystalline aggregates. These studies have invoked the use of the Hall-Petch relationship to describe the behavior; namely

$$\sigma = \sigma_0 + k d^{-1/2} \quad (1-1)$$

where σ represents the fracture strength, d represents the grain size and σ_0 and k are experimental constants.

Using this description as a basis, Cannon (1985) conducted a series of experiments designed to measure the compressive strength of polycrystalline ice. His efforts confirmed that grain size plays the same important role in determining strength in compression as it does in tension. Cannon was able to show that at a high strain rate (greater than 10^{-3} s^{-1}) the compressive strength of ice was six to eight times that found in tension, close to the prediction using Griffith's Theory (Cannon (1985)), that strength in compression is eight times that in tension (assuming the simplest case of compressive fracture).

All these previous studies have been restricted to the study of ice with one predominant grain size. This situation is rarely found in nature and further study to approach nature more closely was needed. This research examines the effect of a bimodal grain size distribution on the compressive strength of ice as a first step in that direction. Establishing the relationship between strength and a mix of grain sizes (possibly more than two) will allow researchers to identify and measure the effect of other variables introduced, such as salinity and/or porosity much more

accurately. This study also examines the strength of polycrystalline (unimodal) samples under high strain rates (10^{-1} s^{-1}) to attempt to find the grain size-strength relationship.

As each of these successive studies is able to build on the knowledge of the previous, we are better able to understand the effects which different structures have on the compressive strength of ice. The more experimental data we record in carefully controlled research, the better able we may be to understand some of the deformation mechanisms in ice that are not completely understood today. Certainly the more information available on the strength of ice will aid the engineer, as he or she is called to make decisions that hinge on ice strength, such as the strength of structures that must withstand the forces exerted by ice or the load-bearing capacity of an ice sheet required to support a structure.

2. BACKGROUND

This chapter reviews work basic to the area of research and looks at the underlying theory that explains the behavior.

2.1 Grain Size Dependence

One well established relationship that has been shown to apply in the mechanics of many materials is the Hall-Petch relationship given in Equation (1-1). Hall (1951) and Petch (1953) initiated the theory with the application specific to mild steel. Armstrong (1970) showed its applicability on other materials in the metallic field. Rice (1972) has demonstrated the use of the Hall-Petch relationship in predicting the strength of ceramics. Muguruma (1969) noted the applicability of the relationship for ice. Currier (1981) and Lim (1983) applied the Hall-Petch relationship as the basis of their research with freshwater polycrystalline ice. Currier (1981) performed tension tests, but was not successful in showing the brittle to ductile relationship that Schulson (1979) had predicted using the Hall-Petch theory as a basis. Lim (1983) expanded the application of the relationship by testing over a range of temperatures and grain sizes and found the relationship accurately described the behavior recorded. Moreover, Lim showed the brittle to ductile transition upon decreasing grain size that was earlier predicted.

Lee (1985) continued the work in this same area and examined the effects under tension at two strain rates. From experiments at -10°C , he was able to clearly show that strength was controlled by crack nucleation at a high strain rate (10^{-3}s^{-1}) and by crack propagation at a lower strain rate (10^{-7}s^{-1}). Throughout this experimentation the Hall-Petch relationship was used to describe the mechanical behavior of the ice.

Cannon (1985) attempted to apply the same relationship to the compressive strength of ice. He was successful in showing its applicability over a range of strain rates from 10^{-6} s^{-1} through 10^{-3} s^{-1} . The basic form of the relationship in the ductile regime as described by Lim (1983), is shown by Equation (1-1), and was confirmed by Cannon (1985). In the brittle regime the same inverse squared correlation between the grain size and strength is found in this relationship, which describes brittle mechanical behavior,

$$\sigma = (YK_{IC})d^{-1/2} \quad (2-1)$$

where σ again represents the strength, Y is a geometrical factor of order unity, K_{IC} , is the fracture toughness, and d is the grain size.

Cole (1985) presented supporting evidence with his investigation of the strength of ice in compression over a range of strain rates. Using the same experimental technique, which allows direct comparison, the results of Cole fit closely to those of Cannon (1985) and Schulson and Cannon (1984). In contrast, Jones and Chew (1983) claim there is no significant grain size dependence on compressive strength based on their experimentation at a strain rate of $5.5 \times 10^{-4} \text{ s}^{-1}$ at (-10°C) , using grains ranging from 0.6 to 2.0 mm. Failure to observe any grain size effect on strength may have been the result of the limited range of their grain sizes or choice of test control. They utilized stroke control and as a result include all the end cap effects in their data.

Michel (1978) reported that in both tension and compression, strength quickly decreases with the increase in grain size and he developed supporting theories. Cole (1985) extended the range of testing to 10^{-2} s^{-1} and was able to demonstrate the inverse square root relationship between grain size and compressive strength was maintained. Although Cole was

working at -5°C and using grain sizes smaller than Cannon, he came to many of the same conclusions. Cole noted not only a definite grain size relationship, but a drop in peak strength as the strain rate increases from 10^{-3}s^{-1} to 10^{-2}s^{-1} . This relationship and drop in strength has yet to be investigated thoroughly at 10^{-1}s^{-1} .

2.2 Law of Mixtures

Recognizing the importance of the structure, specifically the grain size, is an important first step in understanding the mechanical behavior of ice and many other substances. A mix of grain sizes within the material makes the task of predicting the strength of that material more difficult. In ceramics determining the grain size and its effect on strength is a critical task. The inverse square root grain size relationship of Hall and Petch applies in this field as well. Rice (1972) addressed this question in ceramics looking at both tension and compression. Rice pointed out that arriving at a statistical average grain size may not be sufficient, since failure is likely to occur in one of the largest grains (inverse strength relationship). He claims that to insure the strength is projected accurately, the larger grains must be more heavily weighted in determining an average size (average meaning representative).

An attempt to project the strength of an aggregate comprised of a mix of grains was made by Lee (1985). He prepared bimodal samples consisting of varying concentrations of large size ($10 \pm 1 \text{ mm}$) and small size grains ($.6 \pm 0.2 \text{ mm}$) and tested them in tension at 10^{-6}s^{-1} at -10°C . These samples were tested under the same conditions as his unimodal samples. Lee was unable to arrive at any conclusive results, but did hypothesize that the strength of a bimodal grain size distribution could be described

by a linear dependence of fracture strength on the volume fraction. Stated another way, Lee reasoned that a law of mixtures would apply where,

$$\sigma = f_L \sigma_L + (1 - f_L) \sigma_s \quad (2-2)$$

Here σ is the fracture strength of the bimodal sample, σ_L and σ_s are the fracture strengths of large grain and small grain unimodal samples respectively, and f_L is the volume fraction large grain. The small grain volume fraction f_s is not shown since $f_s = (1 - f_L)$. Lee carried this relation one step further by substituting back in the original Hall-Petch equations and derived an expression (in MPa):

$$\sigma = 0.6 + 0.02 \{f_L d_L^{-1/2} + (1 - f_L) d_s^{-1/2}\} \quad (2-3)$$

for ice at -10°C in tension at 10^{-6}s^{-1} where d_L and d_s represent grain size large and the small grains respectively and the values 0.6 (MPa) and 0.02 ($\text{MPa} \cdot \text{m}^{1/2}$) are the experimental constants determined by Currier and Schulson (1982). These values of σ_0 and k must be determined for the appropriate strain rate. This highlights the strain rate dependence of the strength of ice. Values for σ_0 and k in compression can be found in Cannon (1985) over a range of strain rates.

3. PROCEDURE

This chapter contains the methods used in sample preparation, the testing techniques, and the post-test procedures. Also, it addresses the quality of the samples used.

3.1 General Technique

The ice in this research was prepared in the laboratory and tested utilizing the same techniques used by Cannon (1985). Preparation techniques are based on the work of Cole (1979). The result is a right circular cylindrical sample of essentially bubble-free ice with randomly oriented grains throughout the polycrystalline aggregate. There were two sample sizes used, that of Cannon (1985), which is 9.1 cm diam. x 23.1 cm, and a larger sample 10 cm diam. x 32.7 cm. The size of the mold had no effect on strength; results were similar from both. The larger size allowed for the testing of larger grains (insuring the sample diameter was greater than ten grains).

This research builds directly on the work of Cannon (1985) and his results form the foundation on which the present work is based. This required that all techniques in this work to be identical to those of Cannon (1985), with the exception of the bimodal mix of grains within the bimodal samples. This being the case, the technique will not be discussed in detail. This is not to give the impression that the technique was not critical to this work; on the contrary, the ice making technique of Cole (1979), as refined by Lee (1985), is the basis which allows this work and many others to be conducted with confidence.

3.1.1 Equipment Used

The equipment utilized for preparation of ice samples was the same as that used by Cannon (1985) and Lee (1985). A circular hollow mold made from lucite was used to form the right cylinders of ice. The mold had carefully machined alignment caps at each end, which assured the parallelism of the ice top and bottom. Readings from a comparator, discussed further in another section, designed to measure this parallelism, normally indicated a difference of 0.125mm. The ice was frozen to synthane end caps, which were used as end constraints. Figure 3.1 shows a photograph of the lucite mold, alignment caps and end caps. A cooling coil was used to insure that the ice would freeze radially inward. Figure 3.2 shows a schematic of the mold. For a more complete description of the equipment utilized and information on its manufacture see Lee, et al. (1984).

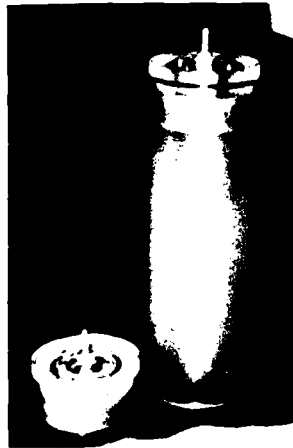


FIGURE 3.1 Photograph of lucite mold, lucite alignment caps with sythane end caps attached. Note hose fittings on both alignment caps and series of O-rings between alignment cap and end cap to make the fit airtight.

3.1.2 Water Preparation

One step in the sample preparation calls for flooding the mold with water and allowing it to flow through the mold slowly, which is at this point filled with seed grains. The water carries out the air and impu-

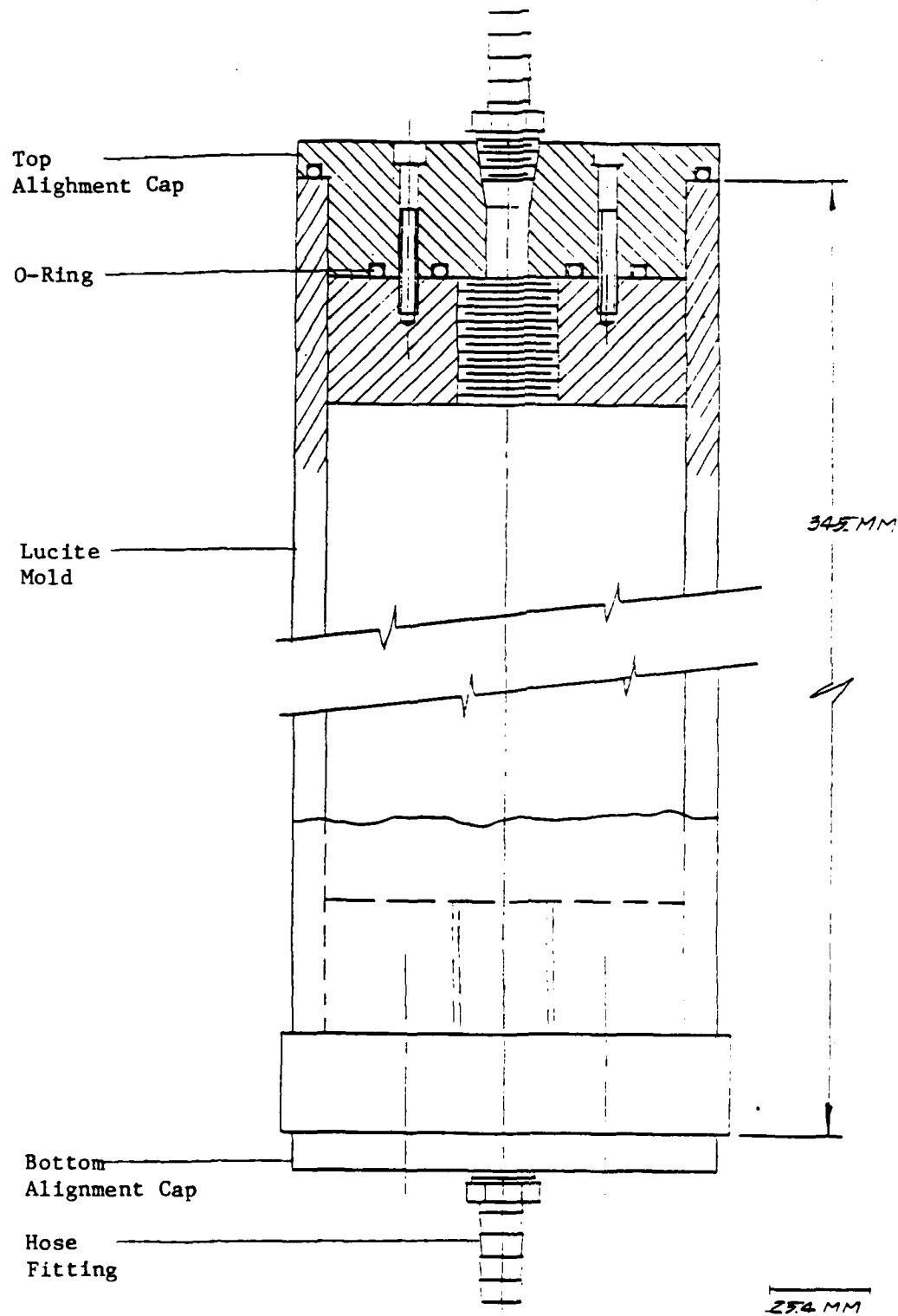


FIGURE 3.2 Schematic Sketch of Molding Apparatus

rities which remain as the freezing front moves radially inward. This water also requires some preparation. Starting with a source of distilled water, the water is treated by a "Nold System", which degasses it while under vacuum. In this distilled, degassed condition the water is drained into the bladder of a sealed water tank. The tank is then placed in a room at 0°C for three days prior to use. Figure 3.3 provides a photograph of the system used to prepare the water for use. Further references for the water treatment can be found in Lee (1985) or Cannon (1985).

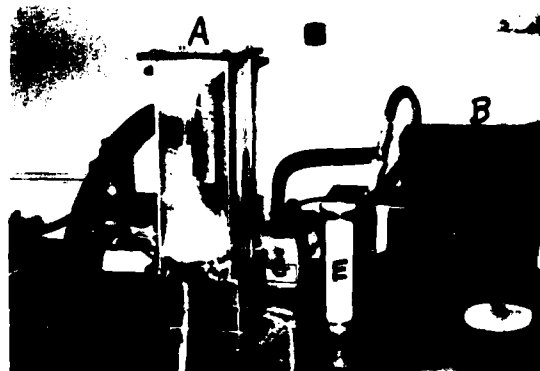


FIGURE 3.3 Equipment for de-airing distilled water. (A) "Nold System" is centered on the table. (B) Cryobath (right rear) prevents water from entering the vacuum pump. Two vacuum pumps are used (rear, left and center). (C) One to evacuate "Nold System" and the second (D) to prepare the water tank (not pictured). (E) Filter tube filled with desiccant.

3.1.3 Seed Grain Preparation

Seed grains were prepared by smashing carefully grown sheets of ice. Pans approximately 30 cm deep were filled with distilled water and placed

in a room at 0°C. Ice sheets whose area averaged 75 cm² slowly grew and were removed. Figure 3.4 shows the pans and a typical sheet of ice. The ice sheets contained few bubbles as a result of the slow formation of ice.



FIGURE 3.4 Ice sheet resting on 30 cm deep ice pan. Note the clear ice and the absence of bubbles. Ice is so thin in the center it cannot be removed in one piece.

The ice sheets were smashed into numerous small grains. The grains were sieved through standard soil sieves, graded by size, and then stored in plastic resealable bags until needed. These bags were stored at -14°C to insure that the grains would remain useable. Figure 3.5 shows a the sieves and the bags of various size seed grains. Cole (1984) provides more information on this seed grain procedure.

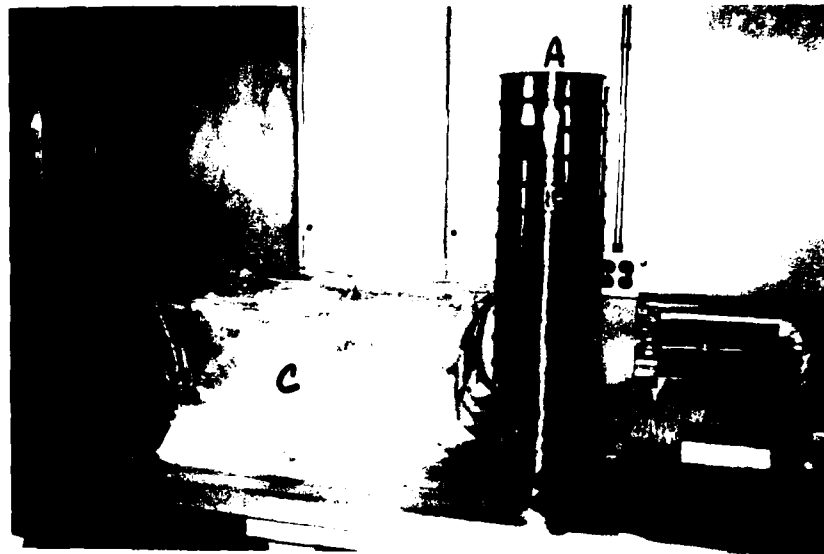


FIGURE 3.5 The standard soil sieves (A) are shown along with rubber mallet and bag, (B) which are used to smash sheets into grains. Resealable plastic bags (C) are shown on the left, with grain size indicated on bag.

3.1.4 Sample Preparation

The sample preparation technique will be quickly reviewed. The result of this work is a right circular cylinder of bubble-free ice. Figure 3.6 shows two samples after removal from the mold. Samples were normally clear, with a very thin cloudy core in the middle, where flow of water was finally frozen.



FIGURE 3.6 Two samples after removal from mold. Note how the sample on the left is cloudy, while the sample on the right is clear ice with cloudiness (fine bubbles) restricted to the central core, the last segment to freeze.

All equipment was allowed to remain in a room at -14°C for a minimum of an hour before starting. The end caps were attached to the alignment caps and placed on the ends of the lucite mold, which was filled with the grains of the desired size (bimodal technique will be discussed later). The sample was now transferred to a room at 0°C . A hose was connected from the base of a sealed tank filled with distilled degassed water to the bottom of the mold. The top of the mold was connected to a vacuum pump and the system was allowed to remain on a vacuum of 2.7 to 6.7 Pa (25-50 millitorr) for three hours before proceeding. Figure 3.7 is a photograph of the setup.

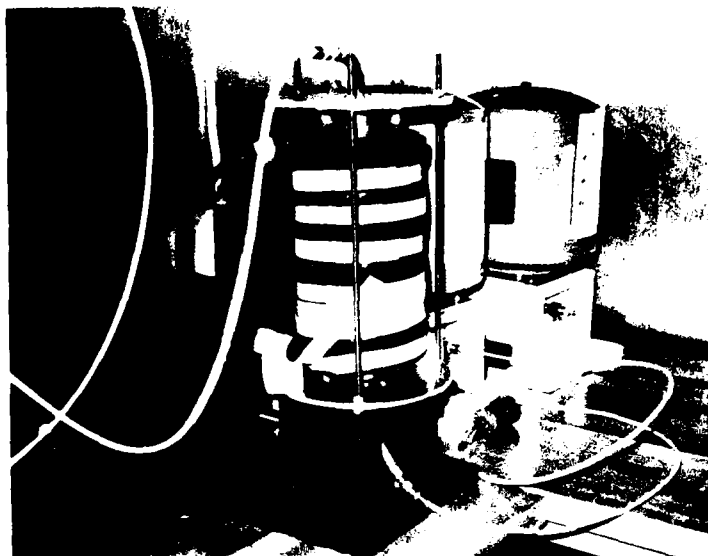


FIGURE 3.7 Only top and bottom of lucite mold can be seen as it sits in the cooling coil. System is on vacuum at this time, with hose connections from water tank to bottom of mold and top of mold to vacuum pump.

At this point the sample was slowly flooded with the degassed distilled water, now at 0°C , and the cooling coil surrounding the mold was turned on at -8°C . The sample was allowed to begin freezing radially inward as the water flowed through the sample and dripped (approximately one drop per second) from the top drain tube. This combination of radial freezing and water running through the core of the mold until it was finally frozen, insured that the sample would have the minimum number of defects and in most cases no bubbles at all. The sample was allowed to freeze for sixteen to eighteen hours. The mold was then removed from the cooling coil and a heat gun used to free the sample. The ice was inspected for quality and transferred to the -14°C room for storage until testing. All samples were wrapped in saran wrap to prevent sublimation during storage. For a more complete description of the process see Lee (1985) or Cannon (1985).

3.1.5 Bimodal Sample Preparation

A challenge in this research was to develop a technique to produce a bimodal distribution of grain sizes. This distribution must be as even as possible throughout the sample and be controlled by the different combinations of large and small grains. Additionally, results from the samples tested must be reproducible. The lack of such a distribution may have been the cause of scatter seen in the data of Lee (1985) when he attempted to test bimodal samples in tension. Figure 3.8 is a photograph of a bimodal sample taken from Lee (1985). Note the lack of an even distribution of large and small grains. At the outset of the project it was decided to maintain consistency and utilize the same grain sizes throughout. The choice of grain sizes was $1.8 \pm .2$ mm (from the 1.7 - 2.0 mm sieve) for the small grain and $5.5 \pm .5$ mm (from the 6.3 - 7.93 mm sieve) for the large grain size. It was hoped that the difference in strength between these two grain sizes would allow for sensitivity and measurement of the grain size effect. An additional consideration was to avoid the disparity in grain size noted by Lee in Figure 3.8, which made the task of an even distribution more difficult. Using two closer grain sizes would have compressed the difference between their respective peak strengths (a significant factor at the lower strain rates) and made quantifying the effect of the bimodal distribution more difficult. Since the grains are produced from ice sheets (explained above), it was soon discovered that lack of fine grains (availability limited by sheet growth, sheet smashing and sieving time) would slow sample production and an additional fine grain ($2.1 \pm .2$ mm) was introduced. This grain was chosen because its strength was very close to that of the aggregate containing $1.8 \pm .2$ mm grains. This choice of two fine grains and one coarse allowed for an

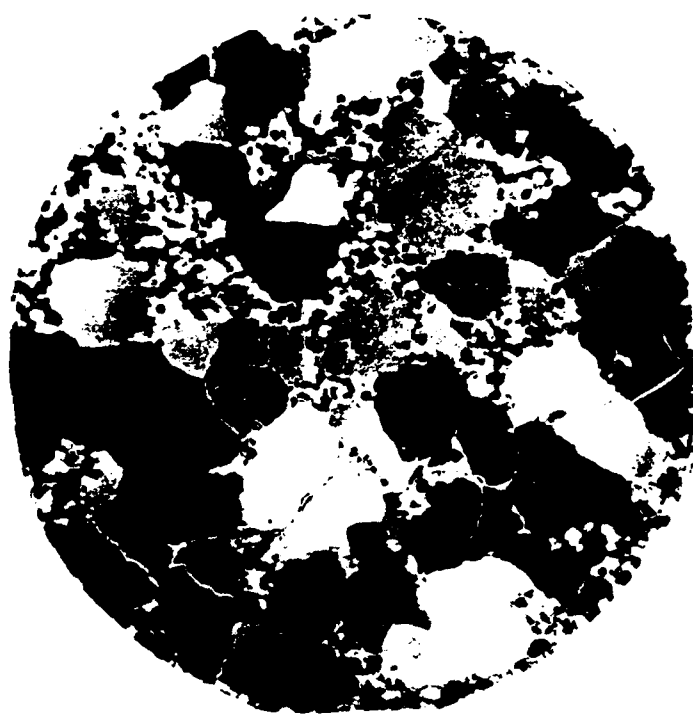


FIGURE 3.8 Thin Section of Deformed Sample with 0.50 Volume Fraction
Large Grain, $\dot{\epsilon} = 10^{-6} \text{ s}^{-1}$, $T = -10^\circ\text{C}$. Large Grain (10 ± 1
mm). Small Grain (0.6 ± 0.2 mm) from Lee (1985)

acceptable level of grain availability and in the end proved a good choice as it expanded the data. Later in the research new sieves were used in the seed grain production and the coarse grain sieve ranged from 6.3 to 8.0 mm, with no effect on large grain size ($5.5 \pm .5\text{mm}$).

The technique used to make bimodal grain size distributions within the sample is simple and direct. The grains were carefully checked to insure all were individual grains and that there were no aggregates within the storage bag prior to use. If aggregates were found, they were crushed, and if extensive, the grains were resieved. Grains were taken from their storage bags, measured by volume, then placed into a third bag in which they were vigorously mixed. This mixing was accomplished by sealing the bag and shaking by hand until the two different size grains were completely mixed. Upon completion of mixing, the grains were then poured into the mold. Great care was taken to insure that an even distribution would result. This required mixing small amounts at a time and using six to nine repetitions of the process before the mold was filled.

3.2 Testing

Testing was conducted at -10°C . Tests using a constant strain rate of 10^{-5}s^{-1} and 10^{-3}s^{-1} were completed at CRREL. Testing was done in an environmentally controlled box affixed to the MTS, which maintained the temperature at $-10^{\circ}\text{C} \pm 1$. The MTS machine at CRREL is a four-posted machine capable of a capacity of 2.2 MN. Strain rate was controlled by the averaged output of two extensometers attached to the endcaps. The system is regularly calibrated and is accurate to 1%. A high speed ink recorder and an X-Y plotter were used to record results. Figure 3.9 shows the CRREL MTS.



FIGURE 3.9 Testing at the CRREL MTS is conducted inside the environmental box at the left. Tests were monitored and photographed through the viewport in the box. Strip chart (A) and x-y recorder (B) are shown on the right.

Tests at a strain rate of 10^{-1} s^{-1} were completed at Thayer School in the Ice Research Laboratory (IRL). The higher strain rate results were recorded on an oscilloscope since x-y recorders were not responsive enough. The MTS is located in a cold room at -10°C , where temperature fluctuation were below 1°C . The IRL MTS is also a four posted machine with a capacity of 489 kN. The cross head can travel over 15 cm/s with 95% of the maximum rated capacity load. It is capable of producing strain rates of approximately 1 s^{-1} on sample sizes that were tested. Tests were done in stroke control as well as strain control (with the averaged output of two extensometers used to control the rate). Figure 3.10 shows a sample being tested with the extensometers mounted on curved rods from test apparatus.

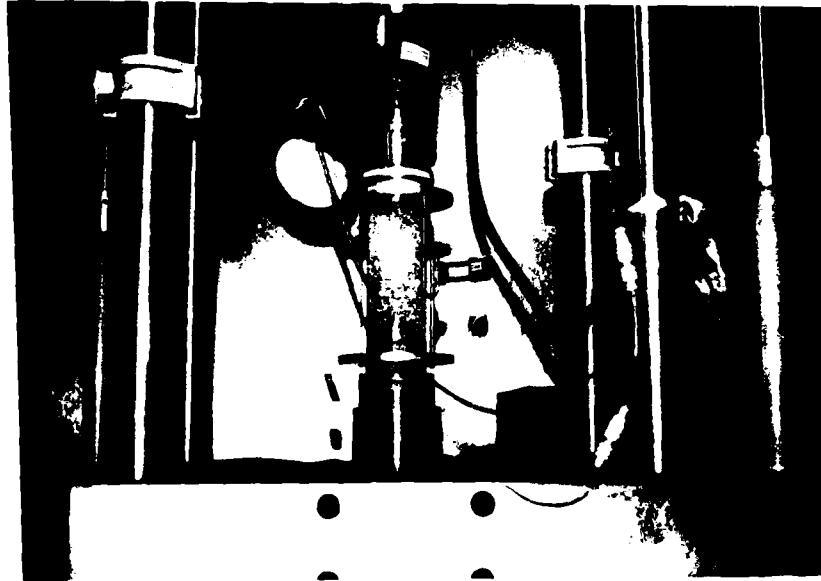


FIGURE 3.10 Sample being tested in compression, from this angle only one extensometer is visible. Note cracks can easily be seen in the sample.

Prior to testing all samples were allowed to stabilize at -10°C . The normal procedure was to insure samples remained at -10°C overnight. Preparation for testing included as a first step an inspection of the sample to visually judge its quality and to find any faults that would cause a questionable test. In most cases when a fault was identified, the strength of the sample was below normal for its grain size or mixture at all strain rates. Following this visual quality inspection, the sample was placed in a comparator to check on the parallelism of the end caps. Figure 3.11 depicts a sample being checked for parallel end caps. In many cases tolerance was below 0.025 mm and no correction was needed. Often a small shim was utilized to insure the alignment was correct. It was found

that in tests where the tolerance exceeded 0.25 mm the strength of the sample would be below expected values.

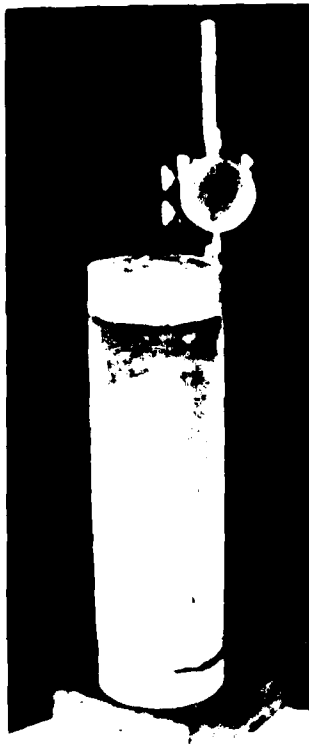


FIGURE 3.11 Sample is measured to determine if top and bottom are parallel. If required, small shims may be used to insure proper testing.

Samples were fitted with a testing apparatus that fit around the end caps (See Figure 3.10). This was attached by thumb screws to the end caps as close to the the ice-end cap interface as possible so as to measure the strain of the ice and not the end cap. Extensometers were connected to curved rods so that as the sample was compressed the extensometers would open, since the device has a greater range in that direction.

Testing events were visually monitored by eye and a number video-taped. Further discussion of testing techniques can be found in Cannon (1985).

3.3 Post-Test Activities

Post test activities included the immediate inspection of the ice after it was tested. Whenever possible samples would be thin sectioned after testing and photographed. The high rate tests did not permit thin sectioning as the ice was too severely cracked. Thick sections were taken on a few of the samples tested at 10^{-5} s^{-1} to assist in looking at crack densities and formation. Elaboration on thin sectioning techniques can be found in Lee (1985). The results of the thin sections allowed an accurate assessment of the bimodal distribution and characterization of the grain sizes involved. Figure 3.12 shows a thin section. Cole (1984) provides a good explanation of the many procedures that can be used for characterization of the thin section.

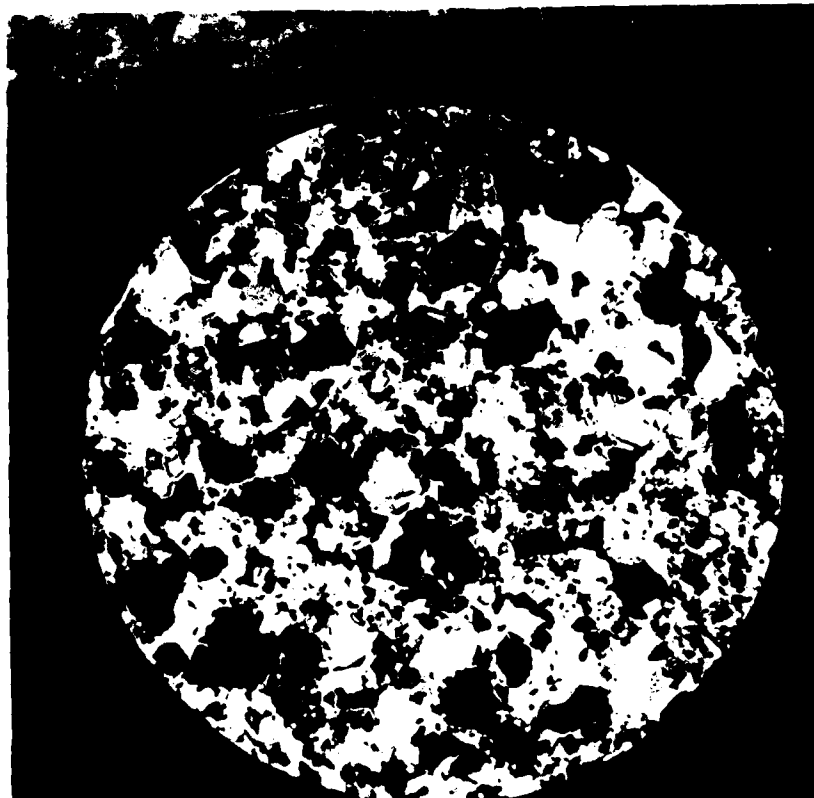


FIGURE 3.12 Thin section of a sample (JL-7) consisting of 50% fine grain ($2.1 \pm .2 \text{ mm}$) and 50% coarse grain ($5.5 \pm .5 \text{ mm}$). Scale is in cm. $T = -10^\circ\text{C}$, strain rate was 10^{-5} s^{-1} .

3.4 Sample Quality

Sample quality was closely monitored by visual inspection after removal from the mold and just prior to testing. The parallelism of the end caps (top and bottom) of the ice was also a major factor in discriminating between good samples and poor ones. The density of the ice used in the experimentation was measured using the displacement method in iso-octane and was found to be the same as Cannon (1985) of $0.916 \pm .001$ gm/cm³ at -5°C. These values are also in agreement with those obtained by others who follow the same preparation techniques.

4. TEST RESULTS

This chapter contains the results from experiments performed on freshwater polycrystalline ice Ih, consisting of equiaxed and randomly oriented grains. Bimodal samples had proportions of large to small grains of 25%/75%, 50%/50%, and 75%/25%, and were tested in compression under constant strain rates of 10^{-5} s^{-1} and 10^{-3} s^{-1} . For comparison the peak stress of unimodal specimens were taken from Cannon (1985) for the strain rate of 10^{-5} s^{-1} . At 10^{-3} s^{-1} , in addition to data provided by Cannon (1985), seven unimodal tests were conducted to confirm unimodal large grain and small grain fracture strength. Unimodal (equiaxed grains) samples were tested at a strain rate of 10^{-1} s^{-1} .

4.1 Bimodal at 10^{-5} s^{-1}

Thirteen experiments were conducted at a strain rate of 10^{-5} s^{-1} . This strain rate allowed post-test analysis of tested samples and confirmation of desired distributions. Photographs of thin sections can be found in Appendix A. Post-test analysis showed actual distributions to be close to desired distribution. This is shown in Figure 4.1, where a photograph of a typical thin section is shown with the desired grain distribution noted below it.

Thin sections completed on specimens tested at a strain rate of 10^{-5} s^{-1} were carefully examined to measure the grain size distribution. Inspection by eye permits determination of the existence of any large aggregates of one type grain and a rough estimate of the distribution. This can be seen from Figure 4.1 and Appendix A.

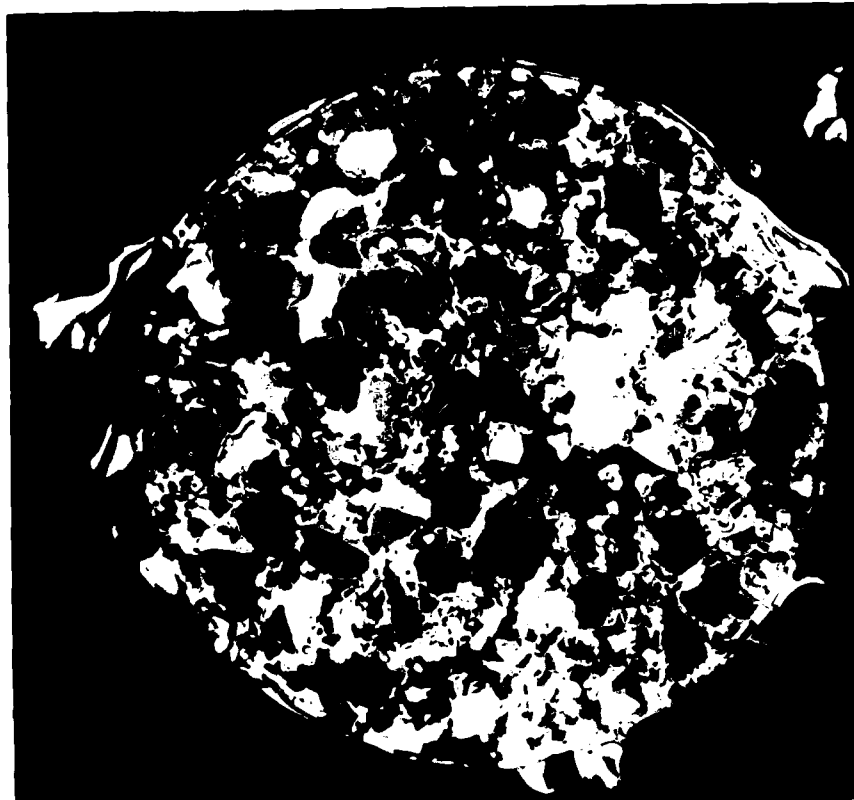


FIGURE 4.1 Thin section of sample (JL-6) bimodal mix of 50% ($1.8 \pm .2$ mm) and 50% ($5.5 \pm .5$ mm). Peak strength was 2.92 MPa. Scale is in cm. $T = -10^{\circ}\text{C}$, strain rate 10^{-5}s^{-1} .

A more accurate measurement of the grain distribution was made for a number of specimens. Thin section photographs were used to reveal a total area of the thin section. Using tracing paper over the photograph, all of the large grains were highlighted and transferred to graph paper. An area was computed for the coverage of the large grains. Results of this examination are shown on Table 4.1. Table 4.1 shows that in all cases the actual distribution is less than the desired distribution. Since thin sections are thinner than the diameter of the large grains, it is to be expected that any measurement of large grain distribution will be less

than actual. This is the result of some large grains appearing as small grains in a specific two-dimensional slice.

Table 4.1 Comparison of Desired vs. Actual Grain Distribution

<u>Specimen #</u>	<u>Desired % Large Grain</u>	<u>Actual % Large Grain</u>
JL-10	25	18
JL-11	25	21
JL-6	50	45
JL-7	50	46
JL-8	75	67
JL-9	75	68

Tests conducted at this strain rate resulted in ductile behavior of all the specimens; i.e stress strain curves continued past a well defined peak and beyond the peak, appeared to maintain a constant slope on the load displacement curve (see stress strain curves in Appendix B). All tests were carried out beyond the peak in the load displacement curve, plotted directly off the x-y plotter of the MTS, and nine were run beyond 30 minutes, i.e. in excess of a strain of 1.8×10^{-2} .

An interesting pattern developed concerning the size of the cracks and the time at which they formed during testing. All samples demonstrated a similar cracking pattern. Specimens developed small cracks first, on order of the size of the small grains, as would be expected from Cole (1984). These small cracks began to appear at a strain of approximately 4.5×10^{-4} , Table 4.2. Cracks initiated individually and became evenly distributed throughout the sample, save the end regions. Once these

cracks appeared throughout the sample, at a strain of approximately 9.1×10^{-4} , large cracks began to appear. Large cracks were estimated by eye to be the same size as the large grains. These large cracks began to increase in number density, while the small cracks continued to appear. After an additional two or three minutes of this activity, i.e. a strain of approximately 2.1×10^{-3} , the sample was so densely cracked that new cracks were difficult to observe. Others who have conducted compression tests (Currier (1981) and Cannon (1985)) have noted that samples were highly cracked and the end zones adjacent to the end caps remained relatively free of cracks.

Table 4.2 Cracking Activity

Sample #	% Large Grain (by Vol)	Time (Strain) to Small Cracks	Time (Strain) to Large Cracks
10	25	1' 10" (.0007)	1' 45" (.00105)
11	25	45" (.00045)	2' 00" (.0012)
12	50	59" (.00059)	1' 40" (.001)
13	50	40" (.0004)	1' 10" (.0007)
14	75	30" (.0003)	1' 00" (.0006)

A quick look at Table 4.1 indicates that the time to small cracks may be a function of volume fraction of large grains. There is not enough data to provide conclusive results.

The strengths (i.e. peak stress) of the bimodal samples tested at the strain rate of 10^{-5} s^{-1} are shown on Table 4.3. Although this study used two fine grains, ($1.8 \pm .2 \text{ mm}$ and $2.1 \pm .2 \text{ mm}$), it can be seen that grain sizes overlap and results will be plotted together. This will be address-

ed further in the analysis. Table 4.3 reflects the bimodal mix, resulting peak stress and corresponding strain at peak stress in the last column. Figure 4.2 depicts a plot of the peak stress versus the volume fraction of large grain ($5.5 \pm .5$ mm). Values for 0% and 100% large grain plotted at the limits are taken from Cannon (1985). Stress-strain curves for these samples can be found in Appendix B.

Table 4.3 Results at Strain Rate of 10^{-5} s^{-1} (-10°C)

No.	Small Grain	Percent (by Vol)	Large Grain	Percent (by Vol)	Strength (MPa)	Strain
8	$1.8 \pm .2$ mm	25	$5.5 \pm .5$ mm	75	2.87	.0021
9	$2.1 \pm .2$ mm	25	$5.5 \pm .5$ mm	75	2.66	.0021
14	$2.1 \pm .2$ mm	25	$5.5 \pm .5$ mm	75	2.58	.0032
6	$1.8 \pm .2$ mm	50	$5.5 \pm .5$ mm	50	2.92	.0041
7	$2.1 \pm .2$ mm	50	$5.5 \pm .5$ mm	50	2.87	.0036
12	$2.1 \pm .2$ mm	50	$5.5 \pm .5$ mm	50	2.70	.0425
13	$1.8 \pm .2$ mm	50	$5.5 \pm .5$ mm	50	2.68	.0036
10	$2.1 \pm .2$ mm	75	$5.5 \pm .5$ mm	25	3.04	.0038
11	$1.8 \pm .2$ mm	75	$5.5 \pm .5$ mm	25	2.97	
2	$3.0 \pm .3$ mm	50	$5.5 \pm .5$ mm	50	2.56	.0024
3	$2.7 \pm .3$ mm	50	$4.3 \pm .2$ mm	50	2.61	.0028
4	$3.0 \pm .3$ mm	50	$6.4 \pm .4$ mm	50	2.51	.0025
5	$1.8 \pm .2$ mm	50	$3.0 \pm .3$ mm	50	3.09	.0042

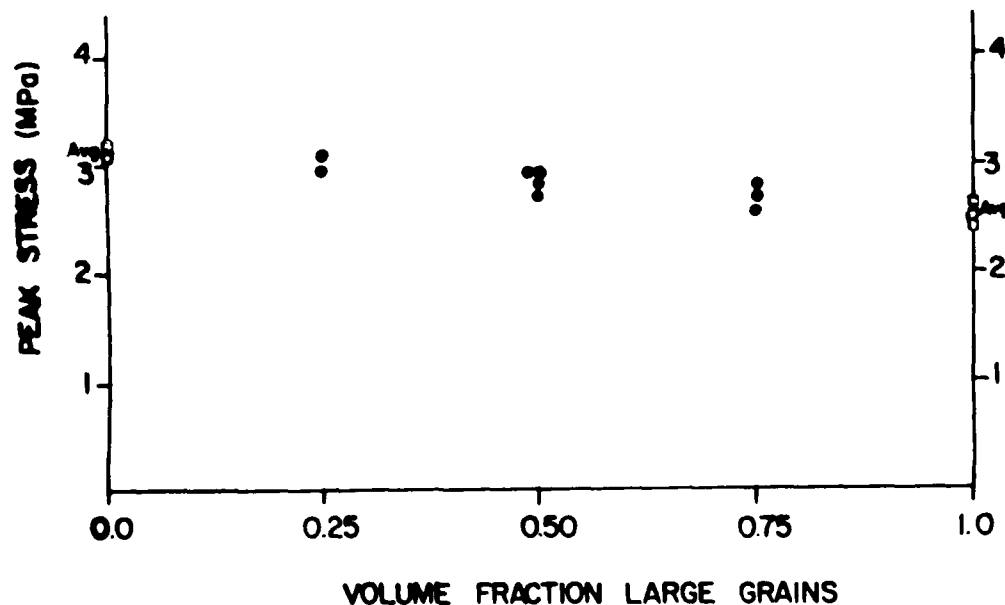


FIGURE 4.2 Peak Stress Plotted Against Volume of Large Grain. Strain rate of 10^{-5} s^{-1} , $T = -10^\circ \text{C}$. (Data reflected by open points are from Cannon (1985))

4.2 Bimodal at 10^{-3} s^{-1}

Twenty-four tests were conducted at a strain rate of 10^{-3} s^{-1} . Testing times were under one second for the usual test. Only one sample behaved in the ductile mode; all others failed in a brittle manner. As expected, the single sample which acted in the ductile manner was the fine grained sample consisting of $100\% 1.8 \pm .2 \text{ mm}$ grains, which was being tested to confirm the value for the fracture strength of the fine grained material. Brittle failures at this strain rate were difficult to categorize. A number failed as described by Cannon (1985), where the result was five large pieces of densely cracked ice and much pulverized snow.

Post-test analysis was limited to photographs of the remaining ice, as thin sections could not be completed on the densely cracked pieces. Other specimens failed in the manner noted by Hawkes and Mellor (1972), described in their discussion of failure in dumbbell versus circular specimens. They classify two major failure types. One as cataclasis, similar to Cannon's observations where conical portions are all that is left intact on the ends attached to the end caps. The other is axial cleavage where large cracks appear to run vertically and the major portion of the ice is intact on one end cap. Hawkes and Mellor (1972) claimed the dumbbell specimens gave higher peak strengths and failed in the cataclasis manner, while the non-tapered cylindrical specimens gave lower peak strengths and failed in the axial cleavage mode. In the present study a difference in strength according to the type failure was not noted. However, both the cataclasis (Cannon's five piece) and axial cleavage type failures were noted. Figure 4.3 shows the results of some samples after testing at 10^{-3} s^{-1} . These photographs show the conical sections as well as large vertical cracks seen in the remaining pieces of ice. Information on samples pictured is listed for convenience.

Table 4.4 Samples Listed in Figure 4.3

No.	Small Grain	Percent (by Vol.)	Large Grain	Percent (by Vol.)	Strength (MPa)
18	$2.1 \pm .2 \text{ mm}$	50	$5.5 \pm .5 \text{ mm}$	50	11.02
19	$1.8 \pm .2 \text{ mm}$	50	$5.5 \pm .5 \text{ mm}$	50	6.92
42L	$1.8 \pm .2 \text{ mm}$	25	$5.5 \pm .5 \text{ mm}$	75	7.12
43L	$2.1 \pm .2 \text{ mm}$	75	$5.5 \pm .5 \text{ mm}$	25	8.75
28L	$1.8 \pm .2 \text{ mm}$	75	$5.5 \pm .5 \text{ mm}$	25	7.05
B-2	$1.8 \pm .2 \text{ mm}$	100		(Ductile)	10.91

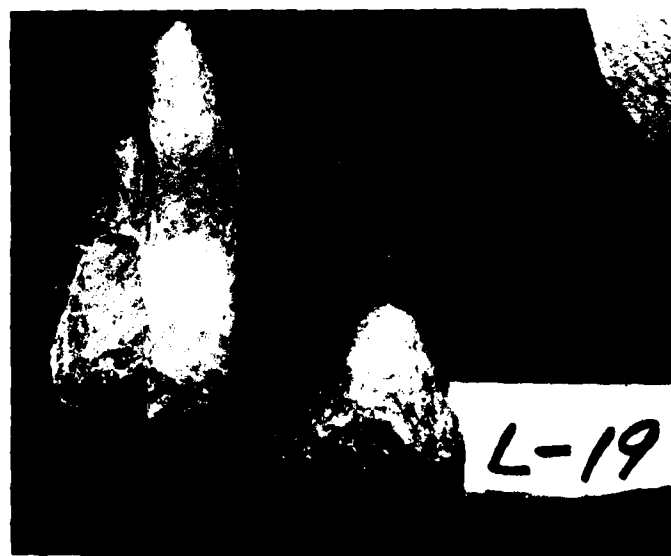


FIGURE 4.3 Results from Testing at 10^{-3} s^{-1} , $T = -10^\circ\text{C}$

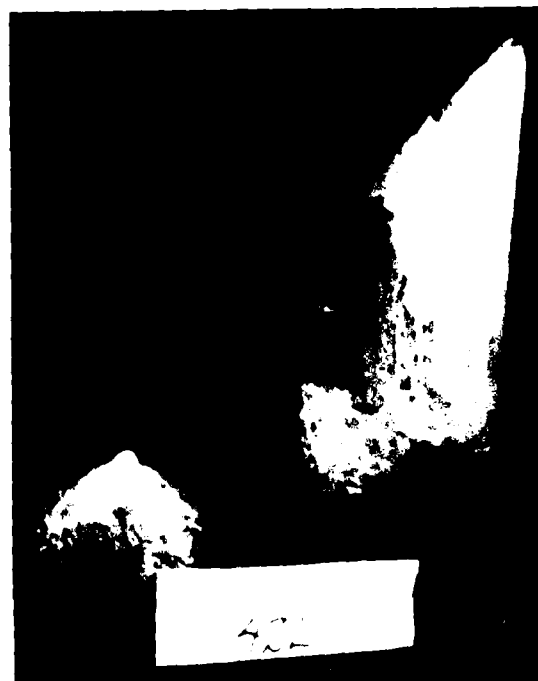


FIGURE 4.3 (cont) Results from Testing at 10^{-3} s^{-1} , $T = -10^{\circ}\text{C}$



FIGURE 4.3 (cont) Results from testing at 10^{-3}s^{-1} , $T = -10^{\circ}\text{C}$. Note one sample behaved in ductile manner - it did not fracture.

Table 4.5 lists the results of tests conducted at 10^{-3}s^{-1} using the same format as Table 4.3. Figure 4.4 graphically shows this same information. The increase in scatter at this strain rate is discussed further in the analysis. Values for the end points were averaged from a number of tests and are plotted along either side of the figure. Two samples were identified as of poor quality prior to testing, as noted on Table 4.5, but all results are plotted for completeness. The resulting values of these two samples will be ignored in data analysis.

TABLE 4.5 Results at a Strain Rate of 10^{-3} s^{-1} (-10°C)

No.	Small Grain Percent		Large Grain Percent		Strength	Strain	Fracture
	(by Vol)		(by Vol)		(MPa)		
15	2.1 ± .2 mm	25	5.5 ± .5 mm	75	6.25	.001	yes
22L	2.1 ± .2 mm	25	5.5 ± .5 mm	75	4.27	.0008	yes
23L	1.8 ± .2 mm	25	5.5 ± .5 mm	75	3.74	.0006	yes*
25L	1.8 ± .2 mm	25	5.5 ± .5 mm	75	7.66	.0012	yes
42L	1.8 ± .2 mm	25	5.5 ± .5 mm	75	7.12	.0012	yes
16	2.1 ± .2 mm	50	5.5 ± .5 mm	50	5.33	.0008	yes
17	1.8 ± .2 mm	50	5.5 ± .5 mm	50	6.83		yes*
18	2.1 ± .2 mm	50	5.5 ± .5 mm	50	11.02	.0017	yes
19	1.8 ± .2 mm	50	5.5 ± .5 mm	50	6.92	.0013	yes
20	2.1 ± .2 mm	50	5.5 ± .5 mm	50	9.47	.0016	yes
21	1.8 ± .2 mm	50	5.5 ± .5 mm	50	7.69	.0016	yes
24L	2.1 ± .2 mm	75	5.5 ± .5 mm	25	4.56	.0016	yes*
26L	2.1 ± .2 mm	75	5.5 ± .5 mm	25	8.87	.002	yes
27L	1.8 ± .2 mm	75	5.5 ± .5 mm	25	9.01	.0018	yes
28L	1.8 ± .2 mm	75	5.5 ± .5 mm	25	7.05	.0016	yes
29L	1.8 ± .2 mm	75	5.5 ± .5 mm	25	6.73	.0016	yes
43L	2.1 ± .2 mm	75	5.5 ± .5 mm	25	8.75	.0018	yes
L-11	2.1 ± .2 mm	100			7.14	.001	yes
L-18	2.1 ± .2 mm	100			7.62	.0017	yes
B-1	1.8 ± .2 mm	100			7.74	.0018	yes
B-2	1.8 ± .2 mm	100			10.91	.0032	no
B-3	2.1 ± .2 mm	100			9.54	.0021	yes
L-10			5.5 ± .5 mm	100	5.16	.0008	yes
L-19			5.5 ± .5 mm	100	4.70	.0008	yes

*Sample 23 and 24 and bubbles present and were noted poor quality prior to test. Sample 17 exceeded the MTS load cell (10 K) and machine shut down prior to total failure. Sample 17 fell apart as it was removed from the MTS. Note sample B-2 acted in a ductile manner, strength reflects yield stress.

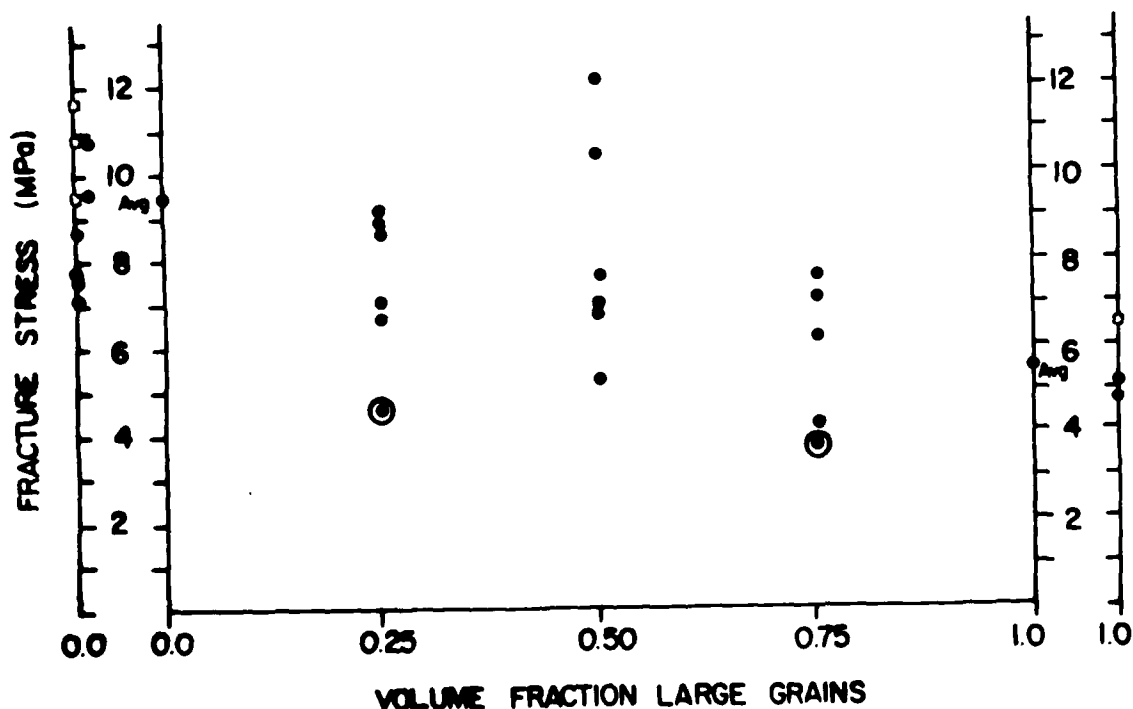


FIGURE 4.4 Fracture stress versus volume fraction of large grain. Strain rate of 10^{-3} s^{-1} , $T = -10^\circ \text{C}$. Sample B-2 (0% large grain) has peak strength plotted as well (10.9 MPa). (Open Figures (\square) depict data points from Cannon (1985))

Careful examination of the stress-strain curves for specimens tested at 10^{-3} s^{-1} , $T = -10^\circ \text{C}$, found in Appendix B, reveals an interesting pattern. In all cases where the volume fraction of large grains is greater than 0.5, the stress-strain plot is a straight line to the fracture stress. In all cases where volume fraction of large grains is less than 0.5, the stress-strain plot reflects some curvature prior to reaching fracture stress. One specimen of 0.0 volume fraction large grain did not fail in fracture and showed a yield stress. This curvature seen in the

stress strain curves, depicting plasticity in the tested specimens, is further proof of Cannon's conclusion that there is a ductile to brittle transition as grain size increases at the strain rate of 10^{-3}s^{-1} , $T = 10^{\circ}\text{C}$.

4.3 Strain at Maximum (Peak or Fracture) Stress

Cannon (1985) noted an interesting relationship between strain at the peak or fracture stress, depending on type of material behavior (brittle or ductile), and the grain size. He showed that this strain (at the peak or fracture stress) decreases with increasing grain size. He also noted that the magnitude of this effect increases with decreasing strain rate. Making use of the stress strain curves found in Appendix B, Figure 4.5 plots strain at peak or fracture stress versus volume fraction of large grain.

It is clear that strain at stress for the specimens tested at a strain rate of 10^{-5}s^{-1} are a factor of two greater than the strain at fracture stress for a strain rate of 10^{-3}s^{-1} . A grain size relationship is difficult to establish, but a similar relationship with the volume fraction of large grains can be seen for the data at 10^{-3}s^{-1} , where strain at fracture stress decreases with increasing volume fraction of large grains.

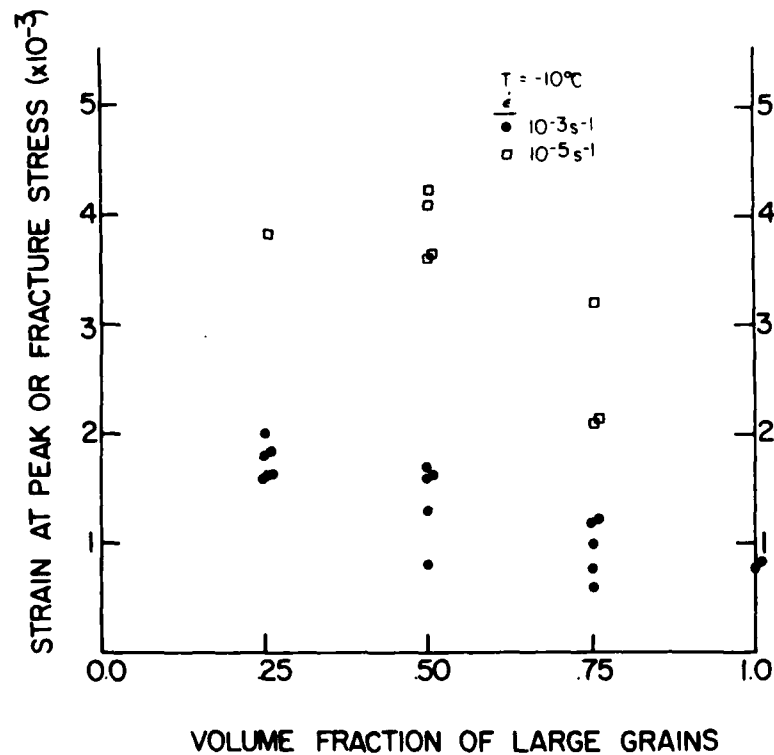


FIGURE 4.5 Strain at Peak or Fracture Stress versus Grain Size, T = -10°C.

4.3 Unimodal at 10⁻¹ s⁻¹

Twenty-three tests were conducted at a strain rate of 10⁻¹ s⁻¹ on samples with grains of one size. Twelve specimens were tested in strain control and the remainder were tested under stroke control. Results of the stroke control tests can be found in Appendix C. The results are difficult to use, since the strain rate is determined only by distance of crosshead travel, which includes strain other than in the ice itself. The results of the strain control experiments are reflected in Table 4.6. This table shows the fracture strengths are below fracture strengths at a strain rate of 10⁻³ s⁻¹. Figure 4.6 is a plot of the data showing fracture stress (MPa) versus the grain size (mm). This figure clearly shows an increase in strength as the grain size decreases.

Table 4.6 Strain Rate of 10^{-1} s^{-1} (-10°C)

No. Sample	Grain Size	Strength (MPa)
L-25	$1.8 \pm .2 \text{ mm}$	5.9
L-29	$1.8 \pm .2 \text{ mm}$	5.7
L-22	$2.1 \pm .2 \text{ mm}$	5.9
L-27	$2.1 \pm .2 \text{ mm}$	5.9
L-32	$2.1 \pm .2 \text{ mm}$	5.8
L-33	$2.2 \pm .2 \text{ mm}$	5.0
L-26	$3.8 \pm .4 \text{ mm}$	5.4
L-28	$5.5 \pm .5 \text{ mm}$	5.0
L-31	$6.4 \pm .4 \text{ mm}$	4.6
L-34	$6.4 \pm .4 \text{ mm}$	4.5
L-23	$8.2 \pm .8 \text{ mm}$	4.1
L-24	$8.2 \pm .8 \text{ mm}$	4.3

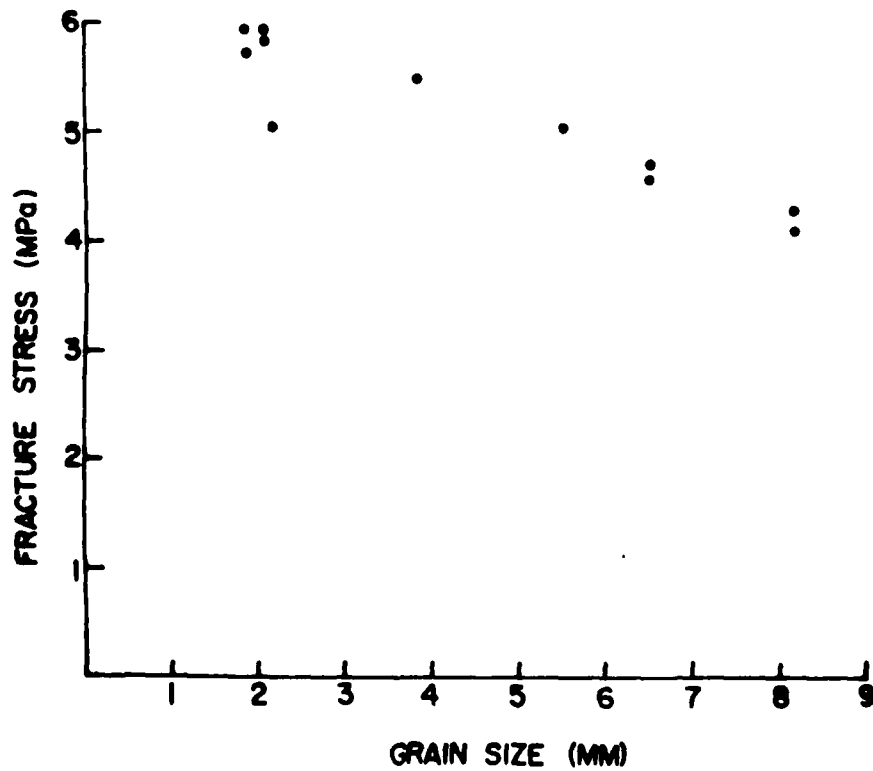


FIGURE 4.6 Fracture Stress vs. Grain Size, Strain Rate 10^{-1} s^{-1} ,
T = -10°C

Once again the test resulted in total destruction of the ice and allowed little post test analysis. Figure 4.7 provides photographs of the end results of a number of these high rate tests. The tests were completed in all cases in milliseconds, with results monitored on an oscilloscope. The oscilloscope is capable of measuring voltage changes in microseconds. The MTS located in the Ice Research Lab was able to generate this constant strain rate with a lag time of approximately one to two milliseconds. The test was over in about ten to twelve milliseconds. These figures come from the load curve and strain curve measured off the oscilloscope. The ice was visibly cracked in all directions, but not nearly as densely cracked as at other strain rates. Large cracks ran vertically in the remaining pieces, while some sizeable portions appeared to have no cracks at all.

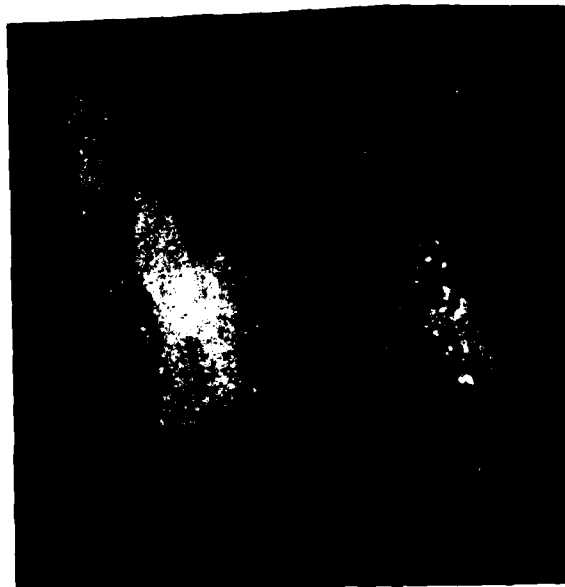


FIGURE 4.7a Results of Testing at 10^{-1} s^{-1} , $T = -10^\circ\text{C}$. Sample 25L Consisting of $1.8 \pm .2 \text{ mm}$ Grains, Fracture Strength 5.9 MPa



FIGURE 4.7b Results of Testing at 10^{-1} s^{-1} , $T = -10^\circ\text{C}$. Sample 29
Consisting of $1.8 \pm .2 \text{ mm}$ Grain Strength of 5.7 MPa



FIGURE 4.7c Results of Test at 10^{-1} s^{-1} , $T = -10^\circ\text{C}$. Sample 22
Consisting of $1.8 \pm .2 \text{ mm}$ Grain Strength of 5.9 MPa

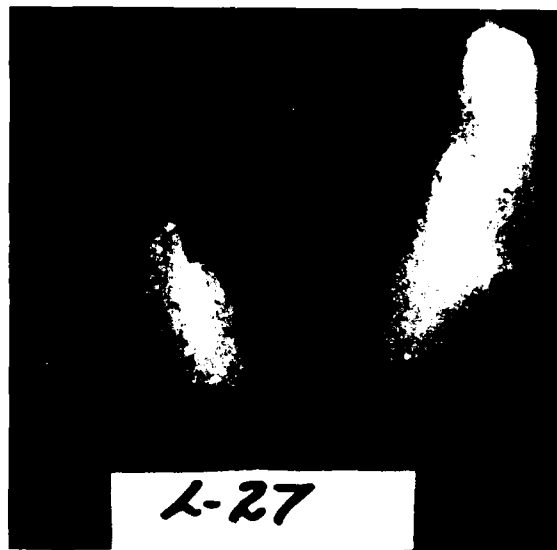


FIGURE 4.7d Results of Test at 10^{-1} s^{-1} , $T = -10^\circ \text{C}$. Sample 27
Consisting of $2.1 \pm .2 \text{ mm}$ Grain Strength of 5.9 MPa



FIGURE 4.7e Results of Test at 10^{-1} s^{-1} , $T = -10^\circ \text{C}$. Sample 32
Consisting of $2.1 \pm .2 \text{ mm}$ Grain Strength of 5.8 MPa



FIGURE 4.7f Results of Test at 10^{-1}s^{-1} , $T = -10^{\circ}\text{C}$. Sample 33
Consisting of $2.2 \pm .2$ mm Grain Strength of 5.0 MPa

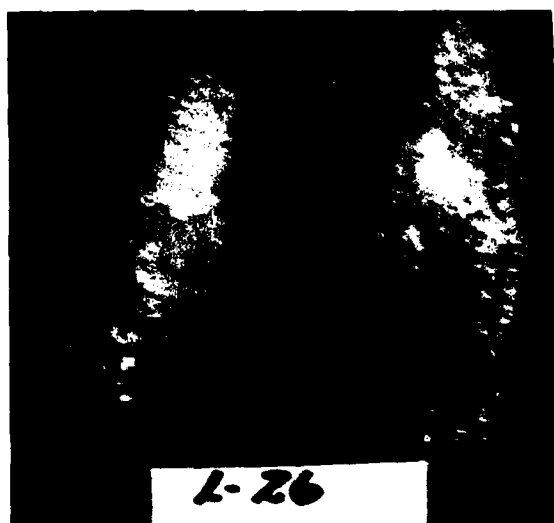


FIGURE 4.7g Results of Test at 10^{-1}s^{-1} , $T = -10^{\circ}\text{C}$. Sample 26
Consisting of $3.8 \pm .4$ mm Grain Strength of 5.4 MPa

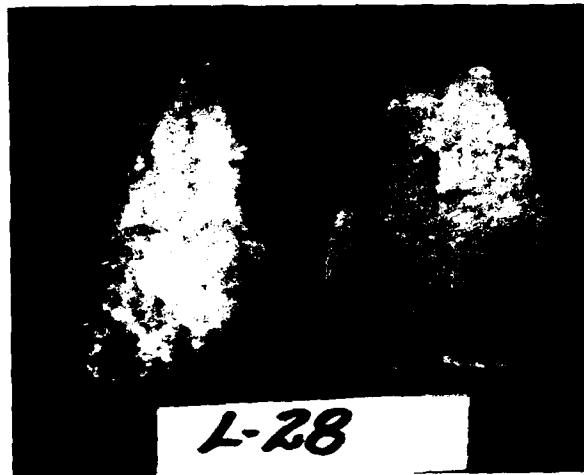


FIGURE 4.7h Results of Test at 10^{-1} s^{-1} , $T = -10^\circ\text{C}$. Sample 28
Consisting of $5.5 \pm .5 \text{ mm}$ Grain Strength of 5.0 MPa

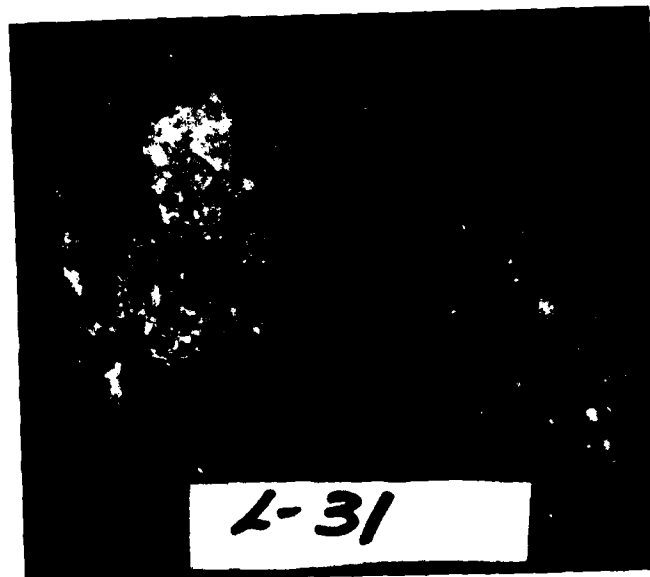


FIGURE 4.7i Results of Test at 10^{-1} s^{-1} , $T = -10^\circ\text{C}$. Sample 31
Consisting of $6.4 \pm .4 \text{ mm}$ Grain Strength of 4.6 MPa

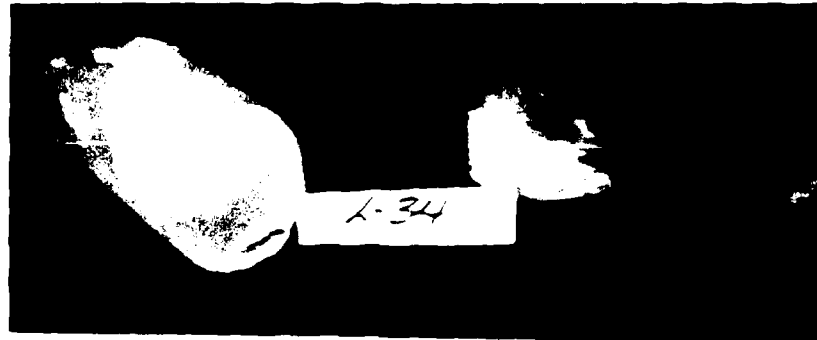


FIGURE 4.7j Results of Test at 10^{-1} s^{-1} , $T = -10^\circ \text{C}$. Sample 34
Consisting of $6.4 \pm .4 \text{ mm}$ Grain Strength of 4.5 MPa



FIGURE 4.7k Results of Test at 10^{-1} s^{-1} , $T = -10^\circ \text{C}$. Sample 34
Consisting of $6.4 \pm .4 \text{ mm}$ Grain Strength of 4.5 MPa



FIGURE 4.71 Results of Test at 10^{-1} s^{-1} , $T = -10^\circ\text{C}$. Sample 23
Consisting of $8.2 \pm .8 \text{ mm}$ Grain Strength of 4.1 MPa

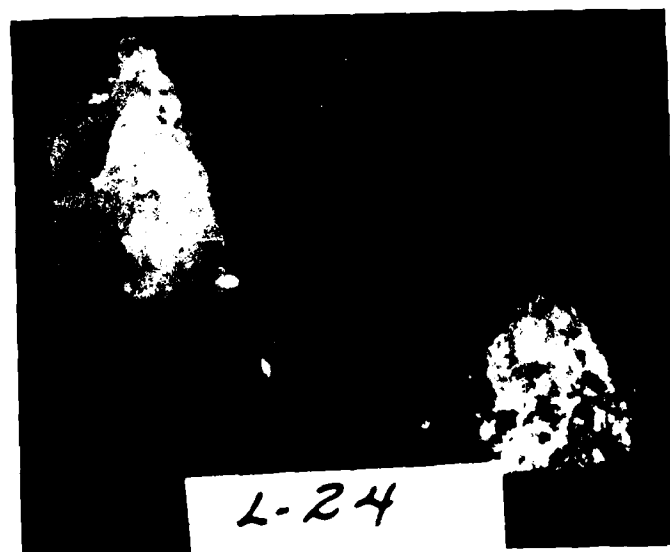


FIGURE 4.7m Results of Test at 10^{-1} s^{-1} , $T = -10^\circ\text{C}$. Sample 24
Consisting of $8.2 \pm .2 \text{ mm}$ Grain Strength of 5.9 MPa

5. ANALYSIS AND DISCUSSION

This chapter provides a detailed analysis of the results and will place the current work in perspective with theoretical models used to describe the behavior noted and other experimental research.

5.1 Cracking Activity

Thin sections were magnified (7X) and photographed in hopes of gaining some insight into crack initiation, propagation or crack stopping. Krell (1981), in studies of bidisperse grain distributions in ceramics (Al_2O_3), noted an improved K_{IC} value and hence a higher fracture strength in bidisperse specimens over unidisperse specimens. This is in direct contradiction to the work of Rice (1972). Krell shows, that for certain bidisperse distributions of large (10-20 μm) and small (2.5 μm) grains, the strength of Al_2O_3 will increase from an average of 375 MPa to over 450 MPa. He claims this is the result of an increase in K_{IC} (fracture toughness) from 5 to 8 ($MPa m^{1/2}$). Krell states that cracks initiate in large grains (in agreement with Rice), but will not immediately propagate through the smaller grains. This cracking, which does not propagate to failure, reduces local stress concentrations and the overall strength is increased. Figure 5.1 is a photograph of a magnified portion (7X) of a thin section. It shows only a small portion of the thin section, but a crack passes from the upper left corner through the lower right side. The crack runs through both size grains. No pattern is detectable. This was an isolated inspection and before any conclusive results are drawn, a more thorough examination is called for. The author was unable to draw any conclusions from the results.



FIGURE 5.1 Photograph of Magnified View of Sample JL-10. Scale along top is in mm. Air bubbles present are the result of mounting thin section on glass slide.

5.2 Law of Mixtures

The main purpose for this research was to determine the effect of a bimodal distribution of grains on the strength of polycrystalline ice in compression. At a strain rate of 10^{-5} s^{-1} at -10°C , it is clear that the peak stress can be determined by the law of mixtures, i.e. Equation (2-2) reproduced here for convenience.

$$\sigma = f_L \sigma_L + (1 - f_L) \sigma_s \quad (2-2)$$

σ is the peak strength of the bimodal sample, σ_L and σ_s are the peak strengths of large and small grain unimodal samples respectively, and f_L

is the volume fraction large grain. Figure 5.2 shows a plot of the data and the predicted strength using Equation (2-2). End point strengths for the 0% ($\sigma_s = 3.06, 3.08$ (MPa)) and 100% ($\sigma_L = 2.72, 2.5, 2.44$ (MPa)) large grain volume fraction were taken directly from Cannon (1985). The data falls close to the the line (predicted strength) with little scatter and proves conclusively, that at this strain rate and temperature, the law of mixtures can be used to predict the compressive strength of ice comprised of a uniform bimodal distribution of grains.

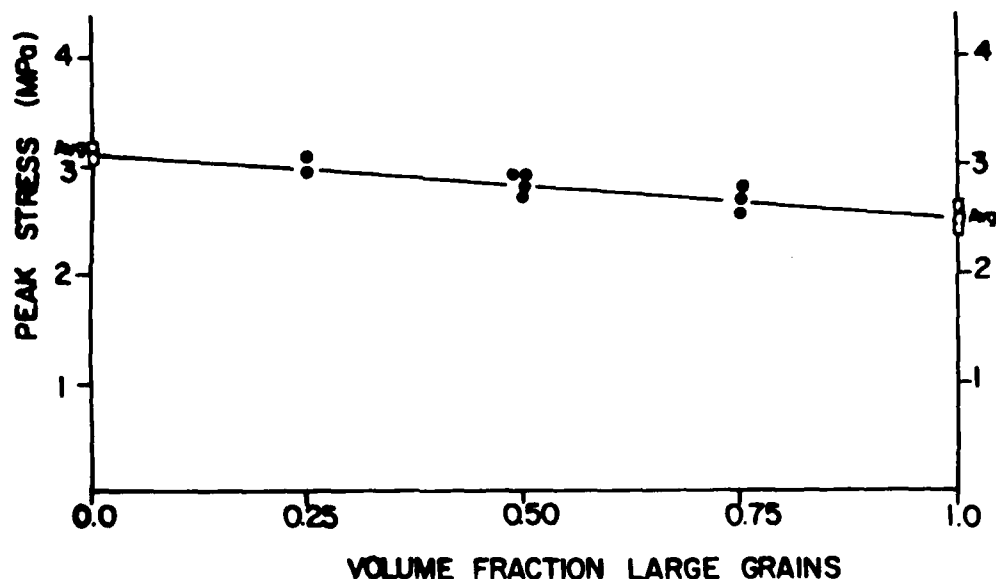


FIGURE 5.2 Peak Stress versus Volume Fraction of Large Grain at a Strain Rate of 10^{-5} s^{-1} , $T = -10^\circ \text{C}$. Line across the figure represents predicted strength from law of mixtures. Data shown by \square are from Cannon (1985).

At the higher strain rate of 10^{-3} s^{-1} an increase in scatter is shown by the results plotted on Figure 5.3. There is scatter in the data at all volume fractions of large grain. This scatter is greater in compression when ice inhibits a brittle behavior, i.e. at a strain rate of 10^{-3} s^{-1} at

-10°C , than the scatter seen at a strain rate of 10^{-5}s^{-1} , -10°C , when ice exhibits a ductile behavior. Now, at 10^{-3}s^{-1} , where strength in compression is controlled by crack propagation (Cannon (1985)), Cannon noted a similar jump in scatter as compared to results from data at strain rates where strength is controlled by crack nucleation. A look at the data of Lee (1985) also shows a significant increase in scatter when strength is controlled by crack propagation. This could be accounted for by some variation in the fracture toughness from one specimen to the next. Moreover, in the specimens comprised of a bimodal distribution of grains, fracture toughness may be effected by the mix, as noted by Krell (1981). While data are limited, this may be the reason for the highest fracture strength at a strain rate of 10^{-3}s^{-1} , -10°C , being recorded at a 50/50 mix of large and small grains.

The line across the figure is the predicted strength from the law of mixtures, i.e Equation (2-2) where $\sigma_L = 5.47 \text{ MPa}$ and $\sigma_S = 9.37 \text{ MPa}$. Fracture strengths for the end points were determined by using the mean fracture strength from twelve tests done by Cannon and the author. One specimen did not behave in a brittle manner and peak strength was used in the average (B-2, 100% 1.8 mm, strength 10.9 MPa).

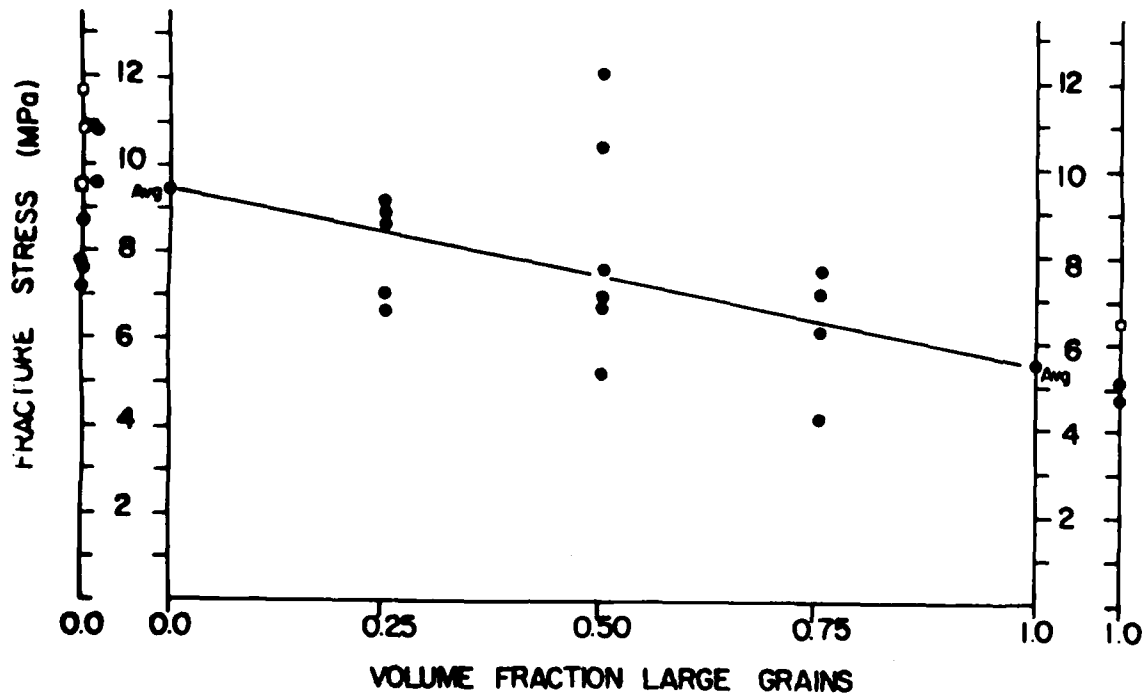


FIGURE 5.3 Fracture stress versus volume fraction of large grains at a strain rate of 10^{-3} s^{-1} , $T = -10^\circ\text{C}$. Line across the figure represents predicted strength for can of mixtures. Data shown by \square are from Cannon (1985).

Statistical analysis of the data at this strain rate shows the mean value for strength at each of the volume fractions of large grain to be very close to the law of mixtures. The greatest difference was noted at the 50%/50% mix, where the mean fracture strength was 0.4 MPa below the strength predicted by the law of mixtures. The standard deviation is plotted versus the volume fraction of large grains on Figure 5.4. It reflects the extent of the scatter at the different volume fraction of large grains. The maximum standard deviation noted was 2.04 MPa at the 50%/50% bimodal mix.

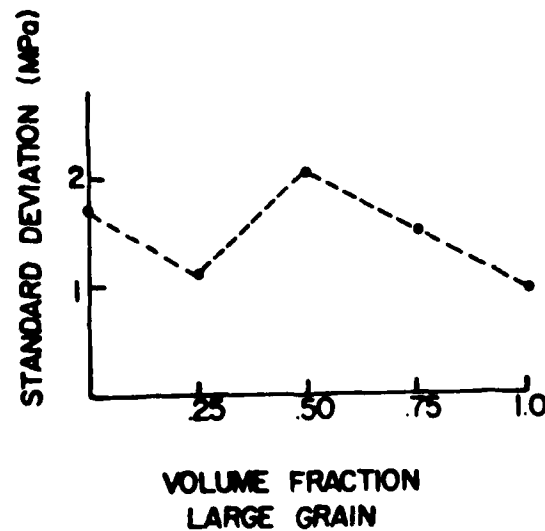


FIGURE 5.4 Standard deviation from data at a strain rate of 10^{-3} s^{-1} , $T = -10^\circ\text{C}$, versus volume fraction of large grains.

This analysis suggests that, at -10°C for the two strain rates examined, the strength of an ice specimen, comprised of a bimodal grain size distribution, has a linear dependence on the volume fraction. This is in agreement with the hypothesis made by Lee (1985), after limited bimodal testing in tension at a strain rate of 10^{-6} s^{-1} at -10°C .

5.3 Significant Grain Size

In the previous section, where the law of mixtures was examined, the strengths for the end points were determined from the result of experimentation. There was no discussion as how to best describe the mechanical behavior of the material. Interest was on strength only. In an attempt to describe the behavior of the polycrystalline ice, it becomes necessary to define certain characteristics of its structure. When testing at a

constant strain rate and temperature, grain size becomes a significant factor in determining the strength for the equiaxed randomly oriented polycrystalline ice. The question then is: What is the equivalent or significant grain size (d_{sig}) of ice, which allows the compressive strength to be calculated for a specimen comprised of a bimodal distribution of grain sizes? This question forces the selection of a specific relationship to describe the strength of ice.

Cannon (1985) invoked the use of the Hall-Petch relationship, Equation (1-1) reproduced for convenience, to describe the behavior for compression at a strain rate of $10^{-5} s^{-1}$ at $-10^{\circ}C$; namely

$$\sigma = \sigma_0 + k d^{-1/2} \quad (1-1)$$

where σ represents the peak strength (MPa), d represents the grain size (m) and σ_0 (1.6 MPa) and k ($0.07 \text{ MPa m}^{-1/2}$) are experimental constants. Using this relationship to determine strength, a substitution is made in Equation (2-2) (the law of mixtures) and the strength of a bimodal specimen in compression at a strain rate of $10^{-5} s^{-1}$, $-10^{\circ}C$ is; (in MPa)

$$\sigma_{bimodal} = f_L (1.6 + 0.07 d_L^{-1/2}) + (1 - f_L)(1.6 + 0.07 d_S^{-1/2}) \quad (5-1)$$

Expanding the right side of this expression;

$$\begin{aligned} \sigma_{bimodal} &= 1.6 f_L + 0.07 f_L d_L^{-1/2} + 1.6 + 0.07 d_S^{-1/2} - 1.6 f_L \\ &\quad - 0.07 f_L d_S^{-1/2} \\ \sigma_{bimodal} &= 1.6 + 0.07 (f_L d_L^{-1/2} + d_S^{-1/2} - f_L d_S^{-1/2}) \\ \sigma_{bimodal} &= 1.6 + 0.07 (f_L d_L^{-1/2} + (1 - f_L) d_S^{-1/2}) \end{aligned} \quad (5-2)$$

This equation (5-2) is in the same form as Equation (1-1) and the values for the experimental constants, σ_0 and k , are equal. Thus

$$d^{-1/2} = (f_L d_L^{-1/2} + (1 - f_L) d_S^{-1/2}) \quad (5-3)$$

Expanding this expression to solve for the significant grain size, which

will be denoted d_{HP} since it is derived from the Hall-Petch relationship, will allow the characterization of a bimodal sample by a single grain size:

$$d_{HP} = \{f_L^2 d_L^{-1} + (1 - f_L)^2 d_S^{-1} + 2f_L(1 - f_L) d_L^{-1/2} d_S^{-1/2}\}^{-1} \quad (5-4)$$

Table 5.1 summarizes the results in determining d_{HP} for each of the bimodal distributions and compares the projected strength Equation (5-2) with the experimental results. Equation (5-2), of course, is only applicable under the conditions of strain rate of $10^{-5} s^{-1}$, and $T = -10^\circ C$.

Table 5.1 Comparison of Projected Strength to Actual Strength

with $d_{sig} = d_{HP}$, at a Strain Rate of $10^{-5} s^{-1}$, $T = -10^\circ C$

Bimodal Distribution	d_{HP}	Projected Strength	Actual Strength
25% Large Grain	2.4 mm	3.02 MPa	3.01 MPa
50% Large Grain	3.0 mm	2.87 MPa	2.79 MPa
75% Large Grain	4.0 mm	2.60 MPa	2.70 MPa

The results allowing $d_{sig} = d_{HP}$ are quite good and the use of the one grain size to compute the compressive strength of the bimodal aggregate is justified.

At the strain rate of $10^{-3} s^{-1}$ at $-10^\circ C$, Cannon (1985) continued to use the same basic relationship, Equation (1-1), although the value for σ_0 was 0. This relationship best describes the mechanical behavior in the brittle zone, where ice exhibits a fracture stress instead of a peak stress. Since the current research doubled the data available at this strain rate, a new regression analysis was completed to determine the best fit for a relationship of the form;

$$\sigma_{bimodal} = kd^{-1/2} \quad (5-5)$$

Figure 5.5 show the fracture stress versus the inverse square root of the grain size for the specimens tested at $10^{-3} s^{-1}$, $T = -10^\circ C$ where d was

computed as d_{HP} . Cannon's data is included for comparison and was also used in determining the best fit for the specimens exhibiting a fracture stress for the relationship above. The value of k which gave the best fit was $0.43 \text{ (MPa m}^{1/2}\text{)}$ and the line using this value of k is plotted on the figure.

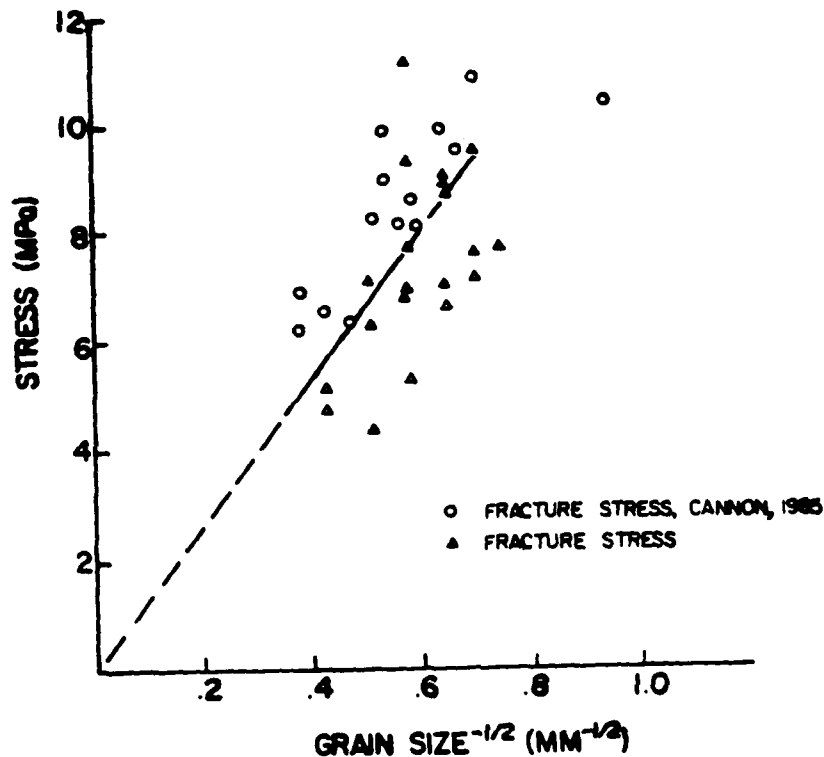


FIGURE 5.5 Fracture Stress versus the Inverse Square Root of the Grain Size for a Strain Rate of 10^{-3} s^{-1} , $T = -10^\circ\text{C}$.

At this strain rate, the same derivation can be used to define d_{HP} and in fact using the same bimodal distributions, yields the same values for d_{HP} . Table 5.2 compares the predicted strengths determined from the use of d_{HP} , in the relationship above (Equation (5-5)), to the actual strengths at the strain rate of 10^{-3} s^{-1} , $T = -10^\circ\text{C}$.

Table 5.2 Comparison of Projected Strength to Actual Strength
with $d_{sig} = d_{HP}$, at a strain rate of $10^{-3} s^{-1}$, $T = -10^{\circ}C$

Bimodal Distribution	d_{HP}	Projected Strength	Actual Strength (Mean Value)
25% Large Grain	2.4 mm	8.77 MPa	8.08 MPa \pm 1.14
50% Large Grain	3.0 mm	7.85 MPa	7.87 MPa \pm 2.84
75% Large Grain	4.0 mm	6.79 MPa	6.33 MPa \pm 1.68

Once again it is evident that the use of d_{HP} is an acceptable method for computing the compressive strength of the bimodal specimen. The fact that this is true does not rule out the use of any other significant grain size. The possibility of using the average grain size (d_{avg}) comes to mind, where;

$$d_{avg} = f_L d_L + f_S d_S \quad (5-6)$$

Allowing $d_{sig} = d_{avg}$ provides the basis for Table 5.3 which compares the predicted strengths of $d_{sig} = d_{HP}$ and $d_{sig} = d_{avg}$ to the actual strengths for a strain rate of $10^{-5} s^{-1}$, $T = -10^{\circ}C$. Note that the value for d_{HP} is smaller than that of d_{avg} .

Table 5.3 Comparison of the Predicted Strengths from
 $d_{sig} = d_{HP}$ and $d_{sig} = d_{avg}$ to the Actual Strengths
for a Strain rate of $10^{-5} s^{-1}$, $T = -10^{\circ}C$

Bimodal Distribution	d_{HP}	Projected Strength	Actual Strength
25% Large Grain	2.4 mm	3.02 MPa	3.01 MPa
50% Large Grain	3.0 mm	2.87 MPa	2.79 MPa
75% Large Grain	4.0 mm	2.60 MPa	2.70 MPa
Bimodal Distribution	d_{avg}	Projected Strength	Actual Strength
25% Large Grain	2.8 mm	2.92 MPa	3.01 MPa
50% Large Grain	3.7 mm	2.75 MPa	2.79 MPa
75% Large grain	4.6 mm	2.63 MPa	2.70 MPa

This table indicates that the use of $d_{sig} = d_{avg}$ leads to a reasonable value for the strength. The results of four tests were not plotted on any previous graphs, because the grains used in the test specimen were outside the sizes established. These specimens will provide a means of verifying the hypothesis that $d_{sig} = d_{avg}$ provides as good a predicted strength as does $d_{sig} = d_{HP}$, outside the limited choice of grains we have discussed up to this point. The samples and their composition are listed in the Table 5.4 below.

Table 5.4 Sample Number and Grain Size Mix

No. Sample	% (by Vol)	Small Grain	% (by Vol)	Large Grain
2	50	3.0 1 .3 mm	50	5.5 1 .5 mm
3	50	2.7 1 .3 mm	50	4.3 1 .4 mm
4	50	3.0 1 .3 mm	50	6.4 1 .4 mm
5	50	1.7 1 .2 mm	50	3.0 1 .3 mm

The use of Equation (5-4) allows us to determine the d_{HP} for each specimen and the d_{avg} is easily computed from Equation (5-6). Table 5.5 is a tabulation of the results of this effort in comparing the predicted strengths of $d_{sig} = d_{HP}$ and $d_{sig} = d_{avg}$ with the actual strengths using Equation (1-1).

Table 5.5 Strengths of d_{HP} and d_{avg} Compared to Experimental
Results for a Strain Rate of $10^{-5} s^{-1}$, $T = -10^{\circ}C$

Sample #	d_{HP} mm	Predicted Strength (MPa)	d_{avg} mm	Predicted Strength (MPa)	Actual Strength (MPa)
2	4.0	2.70	4.3	2.66	2.56
3	3.3	2.81	3.5	2.78	2.61
4	4.2	2.68	4.7	2.62	2.51
5	1.7	3.29	2.4	3.02	3.09

This would indicate that the use of either d_{HP} or d_{avg} would result in a reasonable prediction of compressive strength at this strain rate. Table 5.6 compares the use of $d_{sig} = d_{HP}$ and $d_{sig} = d_{avg}$ in the same manner as above to determine if d_{avg} will provide as good a strength prediction at $10^{-3} s^{-1}$, $T = -10^{\circ}C$. The strengths are determined from Equation (5-5), with $k = 0.43 (MPa m^{\frac{1}{2}})$.

Table 5.6 Comparison of the Predicted Strengths from $d_{sig} = d_{HP}$ and $d_{sig} = d_{avg}$ to the Actual Strengths for a Strain Rate of $10^{-3} s^{-1}$, $T = -10^{\circ}C$

Bimodal Distribution	d_{HP}	Projected Strength	Actual Strength
25% Large Grain	2.4 mm	8.77 MPa	8.08 MPa
50% Large Grain	3.0 mm	7.85 MPa	7.87 MPa
75% Large Grain	4.0 mm	6.79 MPa	6.33 MPa
Bimodal Distribution	d_{HP}	Projected Strength	Actual Strength
25% Large Grain	2.8 mm	8.12 MPa	8.08 MPa
50% Large Grain	3.7 mm	7.06 MPa	7.87 MPa
75% Large Grain	4.6 mm	6.34 MPa	6.33 MPa

At the strain rate of 10^{-3} s^{-1} it is clear that d_{avg} gives a somewhat closer approximation to the experimental results of strength as determined by this study than does d_{HP} . This highlights the effect of the large grains in reducing the compressive strength of the aggregate. The use of d_{HP} will give reasonable results, but in field situations, it would prove much simpler to use d_{avg} than d_{HP} and little is lost in accuracy for the two strain rates investigated at $T = -10^\circ\text{C}$.

5.4 Unimodal Testing at 10^{-1} s^{-1}

Experimentation at this strain rate was conducted under stroke control for approximately half the samples and strain control for the rest. The tests conducted under stroke control, executed much in the same manner as those described by Jones and Chew (1983), provided results that show no relationship between strength and grain size. The results can be found in Table D-1 (Appendix D) and are plotted on Figure D-1. Testing under strain control produced different results. Strengths were, on the average, greater than under stroke control and, from Figure 4.6, a definite grain size-strength relationship can be drawn. The results are similar to the those of Cole (1985), who shows a strength grain size relationship at all strain rates from 10^{-6} s^{-1} through 10^{-2} s^{-1} . This result is also consistent with the findings of all the researchers (Maguruma, Michel, Currier, Lim, et al.) who have shown a grain size dependence on strength. This data is plotted on Figure 5.6 with the fracture stress versus the inverse square root of grain size. Figure 5.6 depicts the data from a strain rate of 10^{-1} s^{-1} and adds Cannon's (1985) results for comparison. Note how this new data mirrors the appearance of that from Cannon at 10^{-3} s^{-1} , with strengths being lower. The plateau

which appears to exist on the right may or may not prove real. Further testing must be done to confirm the behavior at the limits. In addition, testing should be done to insure that constraints imposed by the end caps are not affecting the results, at this strain rate. A strengthening of the ice caused by end cap constraints would make the results appear higher than actual. Conversely, a weakening of the specimen due to constraints may account for the drop in strength from 10^{-3} s^{-1} .

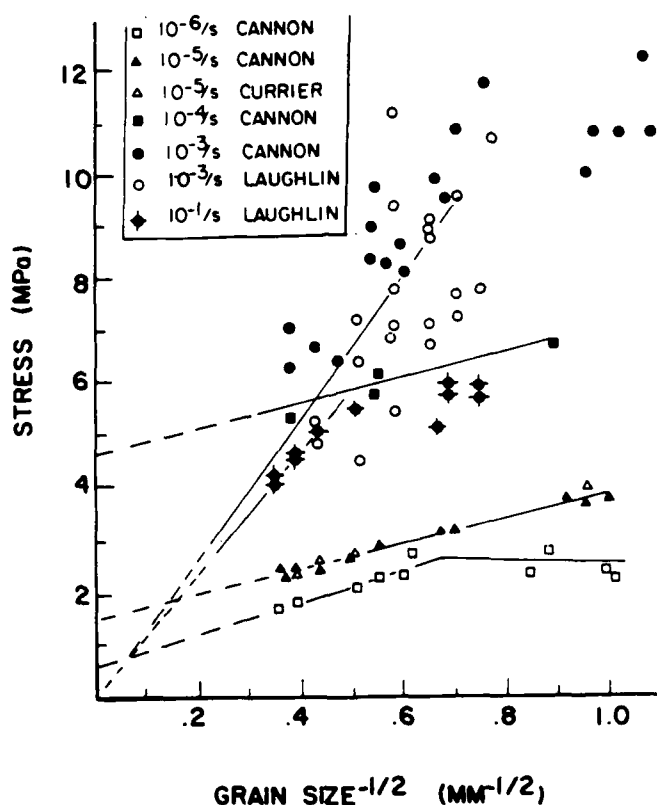


FIGURE 5.6 Stress versus the Inverse Square Root of the Grain size, $T = -10^{\circ}\text{C}$

With the knowledge that this is in the brittle zone and using fracture theory to describe the behavior noted, a curve in the form of Equation (2-1) is appropriate

$$\sigma = (YK_{IC}) d^{-1/2} \quad (2-1)$$

where $k = (YK_{IC})$. The line plotted for the specimens tested at a strain rate of $10^{-1} s^{-1}$, $T = -10^{\circ}C$, on Figure 5.6 represents $k = .37 (MPa m^{1/2})$. This is offered as a best fit for the data shown less than $0.6 (mm^{1/2})$ until the behavior beyond the current limits are investigated.

The results show a drop in fracture strength from a maximum at $10^{-3} s^{-1}$. This is consistent with the results of Cole (1985) who noted a drop in unconfined compression beyond $10^{-3} s^{-1}$ and Jones (1982) who noted a similar drop beyond $5 \times 10^{-3} s^{-1}$, and others (Michel (1978)). Cole and Jones also include plots of log stress versus log strain rate is done here in Figures 5.7 through 5.9 for a number of grain sizes. Cannon (1985) is used as a source of data for the lower strain rates and the current results plotted at $10^{-1} s^{-1}$. Whenever possible Cole's data is also plotted. Note on the figures where both are plotted the similar slope of Cole's results and the combined results of Cannon and the author. There is a slight difference in strength between Cannon and Cole. Cole notes consistently lower strength since he was testing at $-5^{\circ}C$ and possibly, for the larger grain size plotted ($5.5 \pm .5 mm$), Cole was approaching the useable grain size limit of his mold, which is 50 mm wide (or beyond it according to Jones and Chew (1983), who claim the minimum ratio between mold and grain diameter should be 12).

It is generally accepted that in this brittle region deformation mechanisms are elastic in nature, followed by a sudden fracture. This is theorized by Michel (1978) and Cole (1985) appears in agreement. Cannon stated that elastic cracking should dominate the material behavior. He noted the lack of yield points for even the finest grains tested, the obvious brittle fracture of larger grain material and the small strains noted at the peak or fracture stress, depending on specimen behavior.

The drop off in strength beyond 10^{-3} s^{-1} would indicate that at this rate there may be more plasticity involved in the material behavior than Cannon had surmised, and the lack of the plasticity at the higher strain rates accounts for the drop in strength.

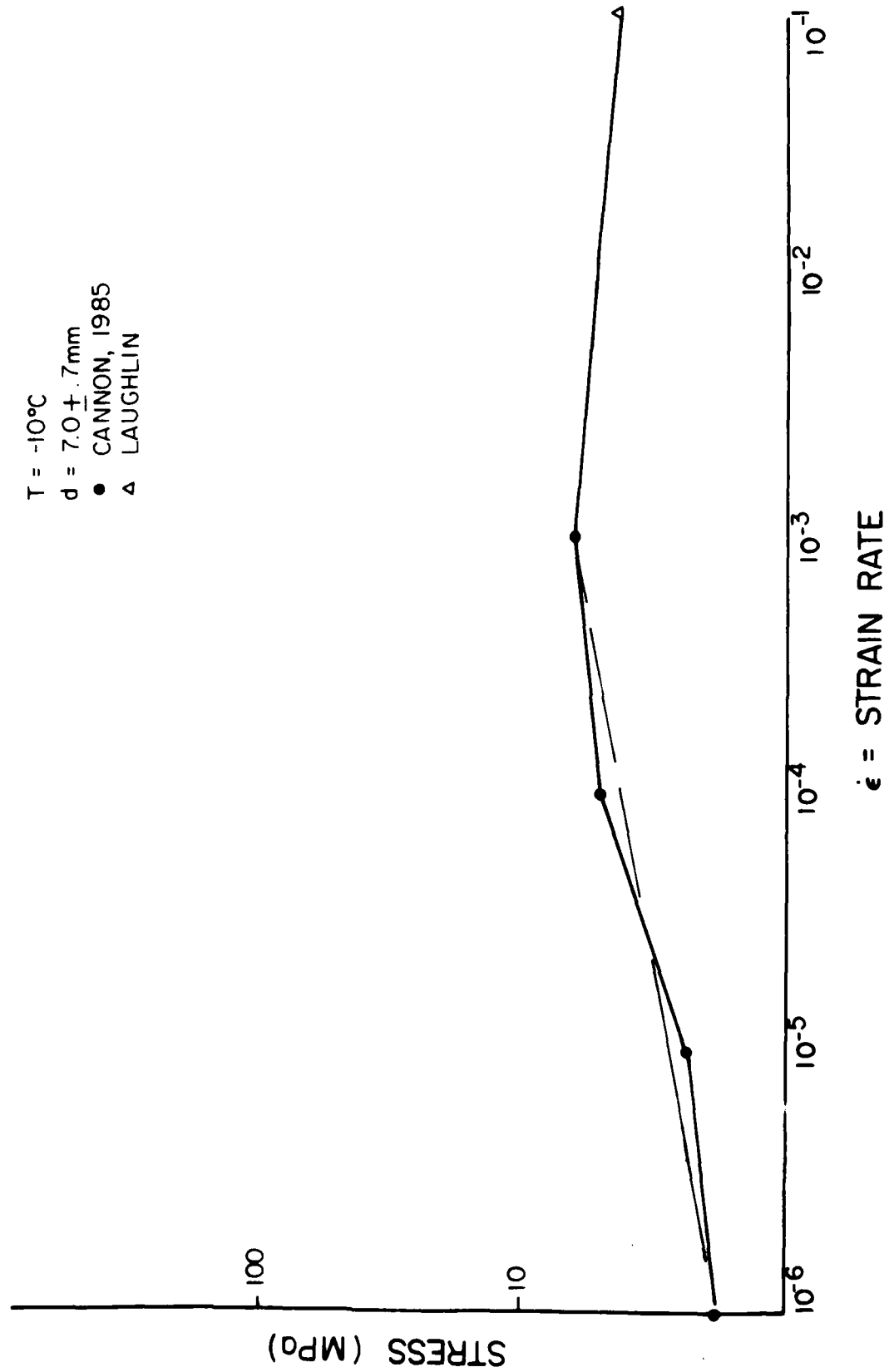


FIGURE 5.7 Log Stress vs. Log Strain for $d = 7.0 \pm 0.7 \text{ mm}$

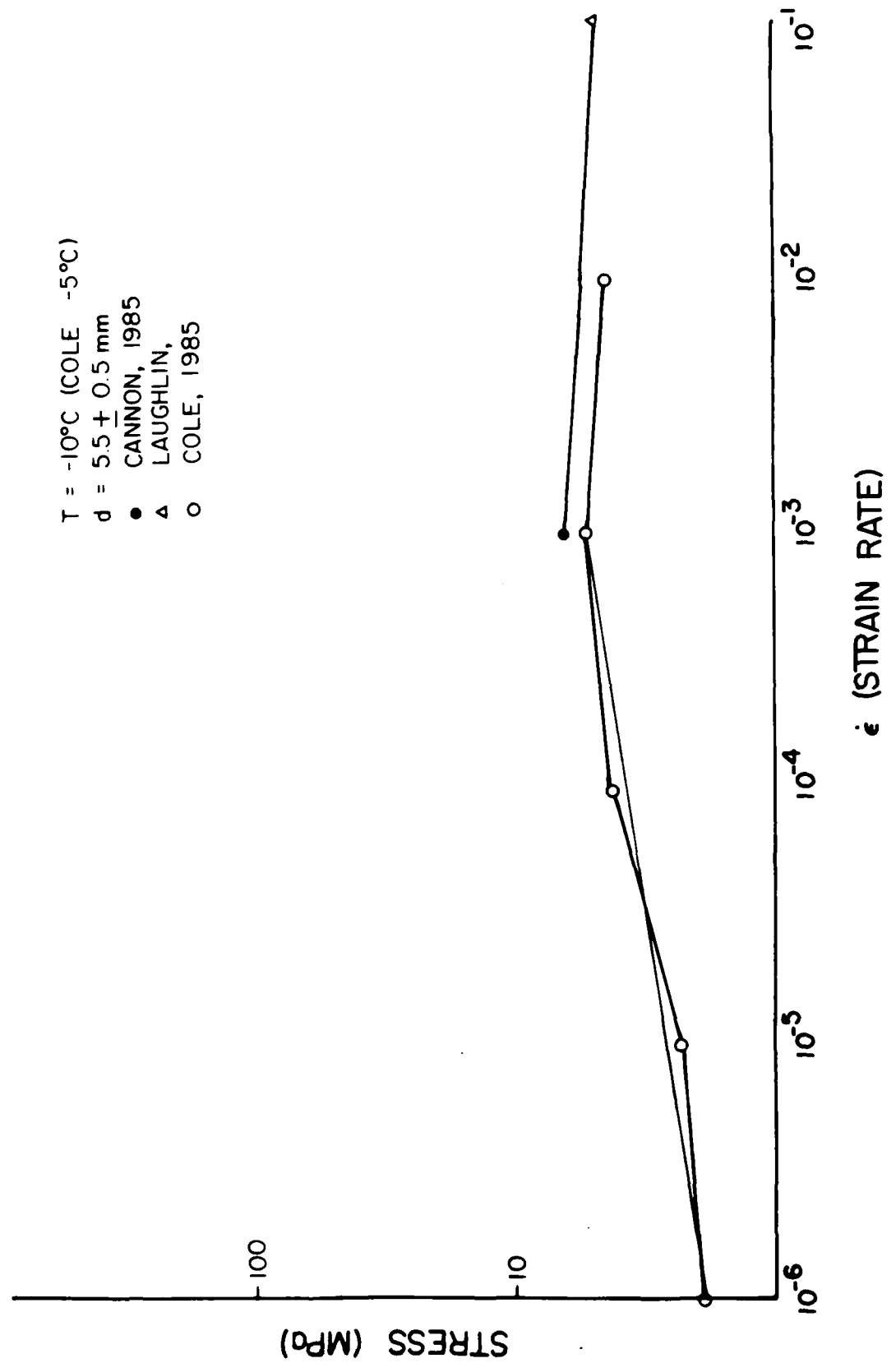


FIGURE 5.8 Log Stress vs. Log Strain for $d = 5.5 \pm 0.5 \text{ mm}$

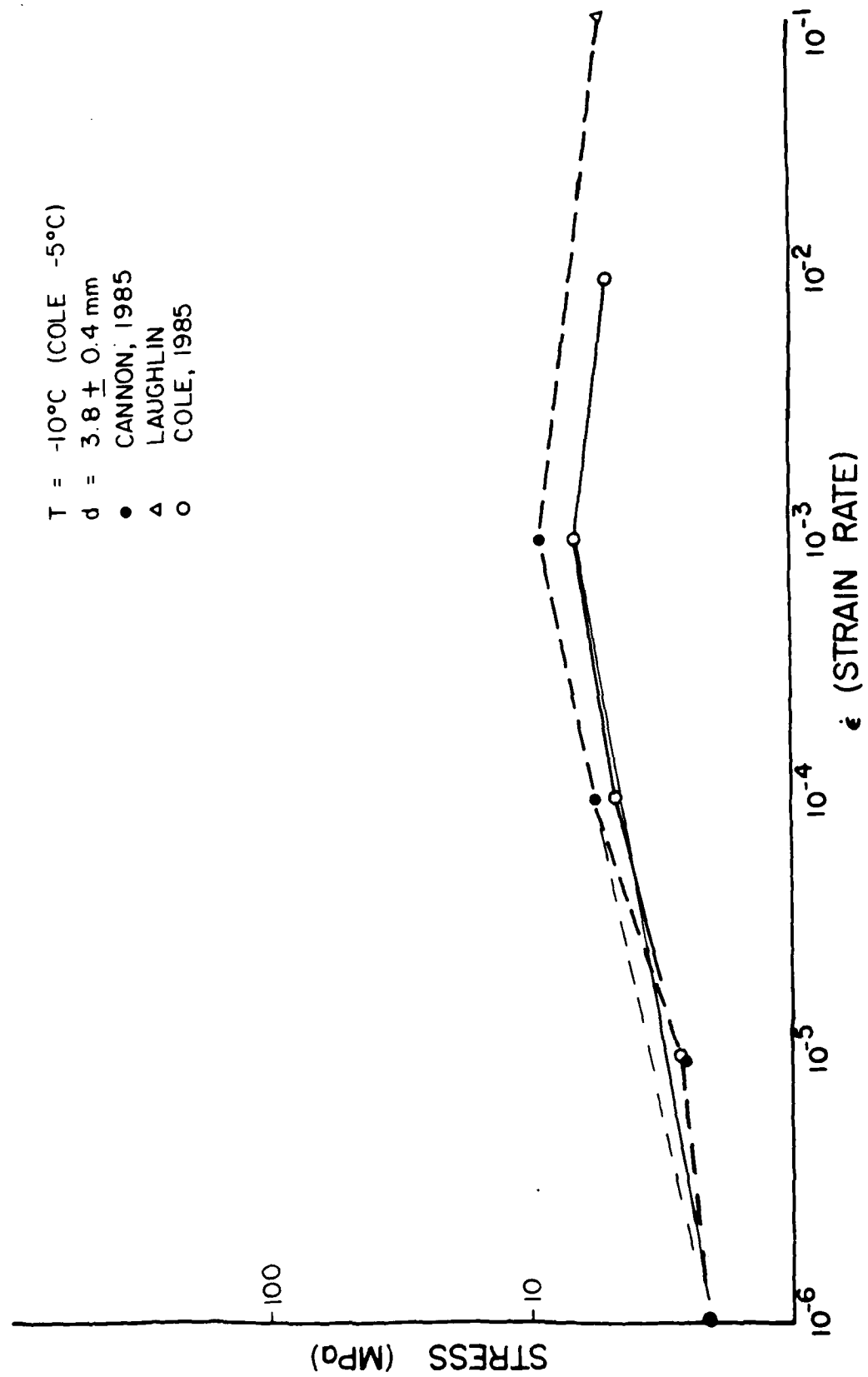


FIGURE 5.9 Log Stress vs. Log Strain for $d = 3.8 \pm 0.4 \text{ mm}$

6. CONCLUSIONS

From experiments at -10°C on the effect of a bimodal grain size distribution on the compressive strength polycrystalline ice at two strain rates (10^{-5}s^{-1} and 10^{-3}s^{-1}) and compression tests on unimodal samples at a strain rate of 10^{-1}s^{-1} it is concluded:

1. The compressive strength of a specimen comprised of a bimodal distribution of grains may be predicted by using the law of mixtures, at strain rates of 10^{-5}s^{-1} and 10^{-3}s^{-1} in the range of grain sizes 2.0 mm to 6.0 mm, where;

$$\sigma_{\text{bimodal}} = f_L \sigma_L + f_S \sigma_S \quad (6-1)$$

2. By invoking the Hall-Petch relationship to describe the mechanical behavior noted, it is possible to define a significant grain size, d_{sig} , where;

$$d_{\text{sig}} = d_{\text{HP}} = \{f_S^2 d_S^{-1} + (1 - f_S)^2 d_L^{-1} + 2f_S (1 - f_S) d_L^{-1/2} d_S^{-1/2}\}^{-1} \quad (6-2)$$

The subscript HP denotes that d_{sig} is computed from the Hall-Petch relation.

3. At strain rates and within the range of grains noted above, the field engineer may find it expedient to use d_{avg} , where;

$$d_{\text{sig}} = d_{\text{avg}} = f_L d_L + f_S d_S \quad (6-3)$$

to represent d_{sig} , with confidence that the resulting strength will be within the range of the standard deviation.

4. At a strain rate of 10^{-1}s^{-1} , under strain control, there is a direct relationship between the fracture stress and the inverse square root of the grain diameter for the range of grains investigated.

5. When the strength of ice is controlled by crack propagation, there is an increase in scatter. Some new mechanisms are involved in determining strength and they related to crack initiation, propagation, and crack stopping.

7. SUGGESTIONS FOR FUTURE RESEARCH

1. An investigation of the cracking pattern noted at a strain rate of 10^{-5} s^{-1} could be accomplished by testing and taking sections (thick or thin) at different strains throughout the test. These sections could provide a great deal of information on crack initiation and perhaps crack propagation. Magnification of thin sections should be carefully studied to determine if any new insights may be gained.
2. The increased scatter noted in compression tests at the higher strain rates may be the result of sample quality, the increasing importance of end cap constraints, or a function of both. A careful study should be undertaken to attempt to reduce the end cap constraints and, in so doing to reduce the scatter and/or isolate the cause.
3. The existence of a relationship between grain size and compressive strength at a strain rate of 10^{-1} s^{-1} is clearly established in a limited range of grain sizes plotted here. There should be further testing at the extreme limits of grain size. Once the grain size relationship is established, bimodal testing should be begun to establish the effect of a grain size distribution on the compressive strength at this higher strain rate.

8. REFERENCES

- Armstrong, R.W. 1970. The influence of grain size on several mechanical properties of materials. *Met. Trans.*, vol. 1, pp. 153-159.
- Cannon, N.P. 1985. The influence of grain size on compressive strength of polycrystalline ice. M. Sci. Thesis. Thayer School of Engineering, Dartmouth College.
- Cole, D.M. 1979. Preparation of polycrystalline ice specimens for laboratory experiments. *Cold Reg. Sci. and Tech.*, vol. 1, no. 2, pp. 153-159.
- Cole, D.M. 1984. The effect of grain size on the internal fracturing of polycrystalline ice. M. Sci. Thesis. Thayer School of Engineering, Dartmouth College.
- Cole, D.M. 1985. Grain size and the compressive strength of ice. *Proceedings of the Fourth International Offshore Mechanics and Arctic Engineering Symposium*.
- Currier, J.H. 1981. The brittle to ductile transition in polycrystalline ice under tension. M. Sci. Thesis. Thayer School of Engineering, Dartmouth College.
- Currier, J.H. and E.M. Schulson. 1982. The tensile strength of ice as a function of grain size. *Acta. Metall.*, vol. 30, pp. 1511-1514.
- Hall, E.O. 1951. *Proc. Phys. Soc. London*, vol. B64, p. 747.
- Hawkes, I and M. Mellor. 1972. Deformation and fracture of ice under uniaxial stress. *Journal of Glaciology*, vol 11, no. 61, pp. 103-131.
- Hobbs, P.V. 1974. *Ice Physics*. Clarendon Press, London, 873 p.
- Jones, S.J. and H.A.M. Chew. 1983. Effect of sample and grain size on the compressive strength of ice. *Annals of Glaciology*, no. 4, pp. 129-132.
- Krell, A. 1981. Alumina structure with improved fracture properties. *Phys. Stat. Sol. (a)*, 63 , pp. 183-192.
- Lee, R.W. 1985. The effect of grain size on the tensile strength of ice at two strain rates. M. Sci. Thesis, Thayer School of Engineering, Dartmouth College.
- Lee, R.W., J.H. Currier, P.N. Lim and E.M. Schulson. 1984. A procedure for testing polycrystalline ice in uniaxial tension. *Journal of Glaciology*, vol. 30, no. 105, pp. 246-247.

- Lim, P.N. 1983. The effects of temperature and grain size on the tensile strength of ice. M. Sci. Thesis. Thayer School of Engineering, Dartmouth College.
- Michel, B. 1978. The strength of polycrystalline ice. Canadian Journal of Civil Engineering, vol. 5, no. 3, pp. 285-300.
- Muguruma, J. 1969. Effects of surface condition on the mechanical properties of ice crystals. Appl. Phys. (J. Phys. D.), Serial 2,2:1517-1525.
- Petch, N.J. 1953. J. Iron Steel Inst., vol. 174, p. 25.
- Rice, R.W. 1972. Strength/grain-size effects in ceramics. Proceedings of the British Ceramic Society, no. 20, pp. 205-257.
- Schulson, E.M. 1979. An analysis of the brittle to ductile transition in polycrystalline ice under tension. Cold Reg. Sci. and Tech., vol. 1, pp. 87-91.
- Schulson E.M. and N.P. Cannon. 1984. The effect of grain size on the compressive strength of ice. Proceedings of the IAHR Ice Symposium, Hamburg, Germany.
- Schulson, E.M., P.N. Lim and R.W. Lee. 1984. A brittle to ductile transition in ice under tension. Phil. Mag. A, vol. 49, no. 3, pp. 353-363.

APPENDIX A

Appendix A provides a collection of thin section photographs.

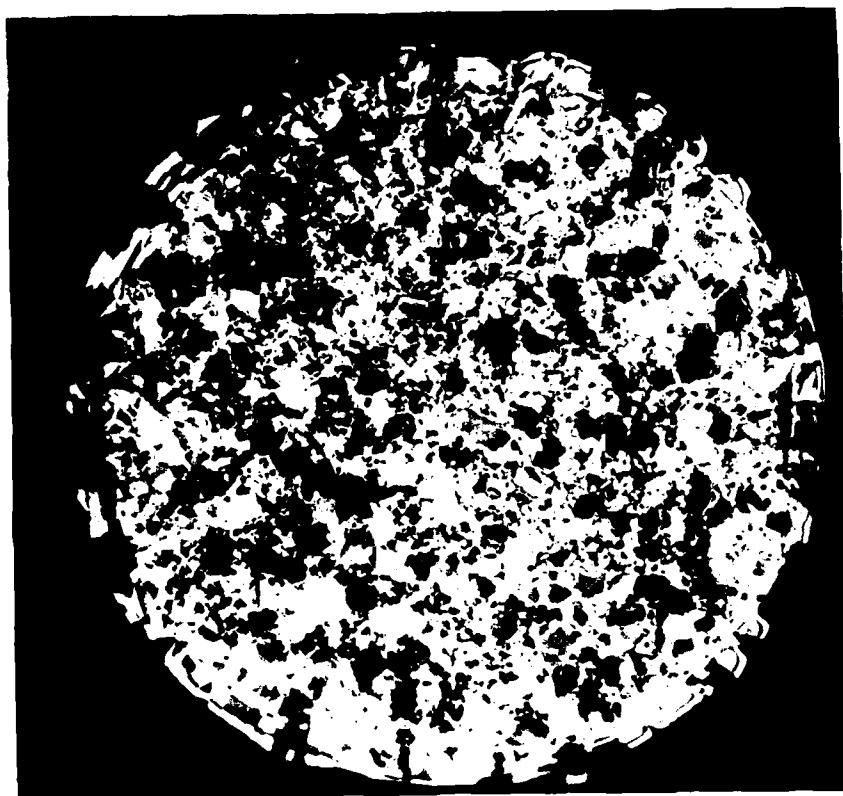


FIGURE A-1 Specimen JL-5: 50% $1.8 \pm .2$ mm
50% $3.0 \pm .3$ mm
Strength at 10^{-5} s^{-1} is 3.09 MPa

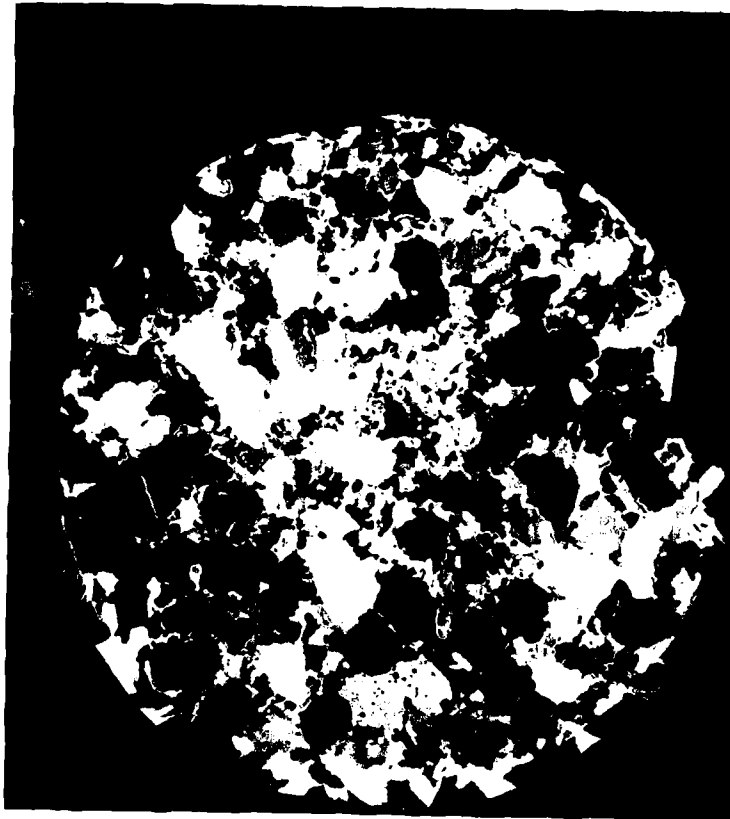


FIGURE A-2 Specimen JL-9: 25% $2.1 \pm .2$ mm
75% $5.5 \pm .5$ mm

Strength at 10^{-5} s^{-1} is 2.66 MPa



FIGURE A-3 Magnification of Thin Section (7X)
Specimen JL-9: 25% $2.1 \pm .2$ mm
75% $5.5 \pm .5$ mm
Strength at $10^{-5} s^{-1}$ is 2.66 MPa

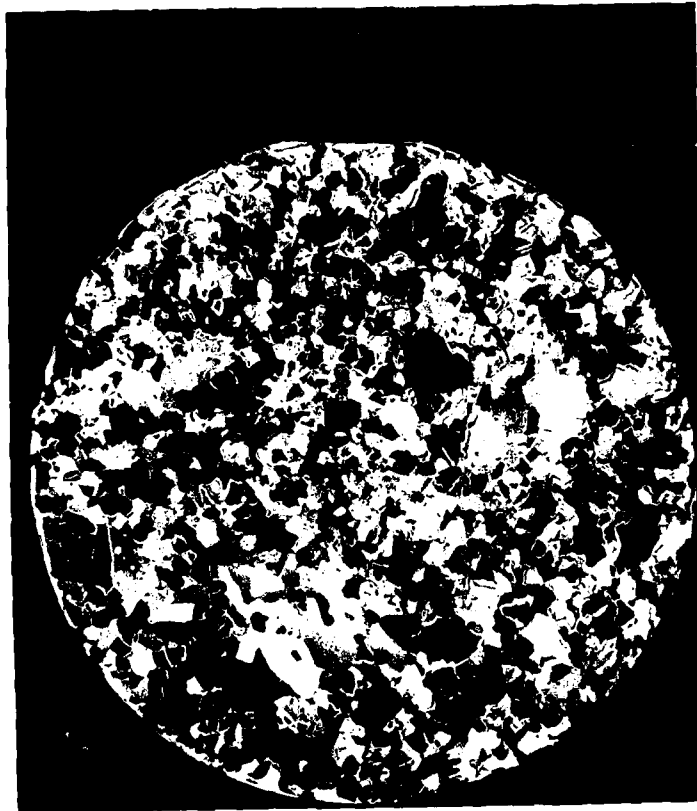


FIGURE A-4 Specimen JL-10: 75% $2.1 \pm .2$ mm
25% $5.5 \pm .5$ mm

Strength at 10^{-5} s^{-1} is 3.04 MPa

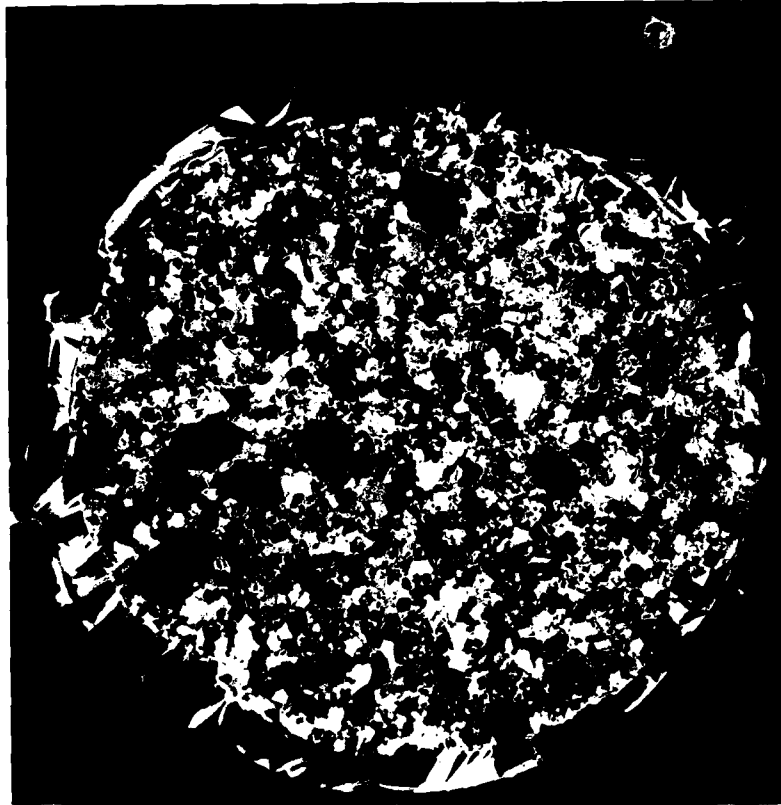


FIGURE A-5 Specimen JL-11: 75% $1.8 \pm .2$ mm
25% $5.5 \pm .5$ mm

Strength at $10^{-5} s^{-1}$ is 2.97 MPa

APPENDIX B

Appendix B contains stress train curves for tested specimens. Samples designated from JL-2 through JL-14 were tested at the strain rate of 10^{-5} s^{-1} . Three samples were tested just beyond the peak, on the load-displacement provided directly from the MTS, all others were tested beyond 30 minutes. The remaining samples in this section were tested at a strain rate of 10^{-3} s^{-1} . The symbols below are reflected on the stress strain curves to indicate either test stopped or sample fractured.

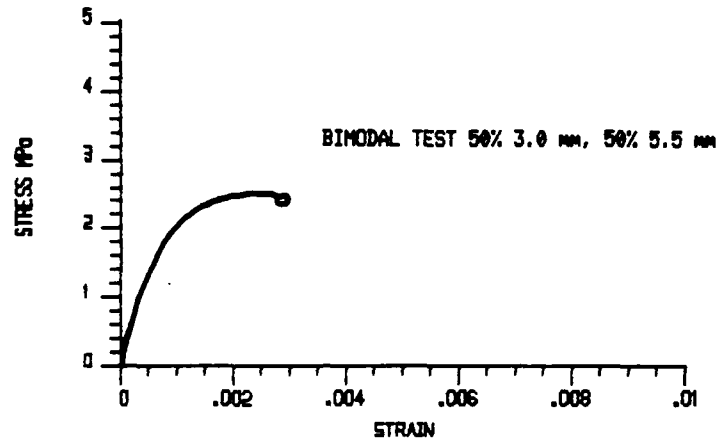
X - sample fractured.

O - test was stopped and sample unloaded.

For those specimens tested in excess of 30 minutes, a diagram of the stress strain curve is shown for the complete test.

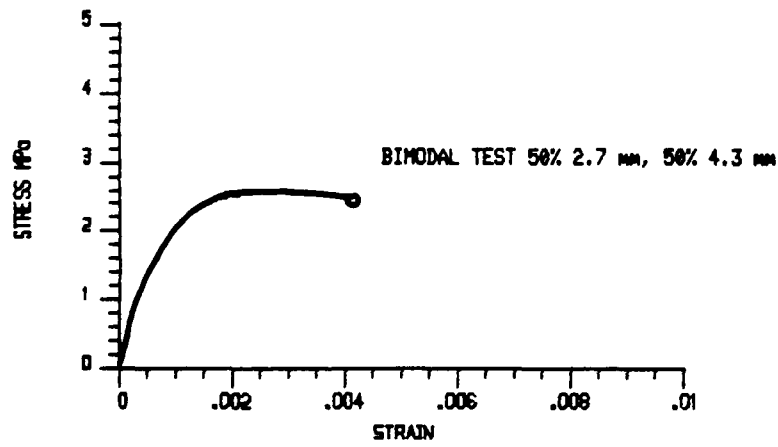
Ready

COMPRESSION TEST JL-2



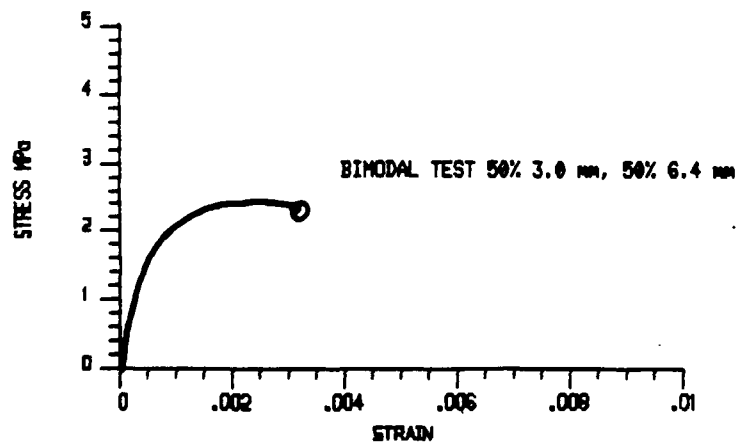
Ready

COMPRESSION TEST JL-3



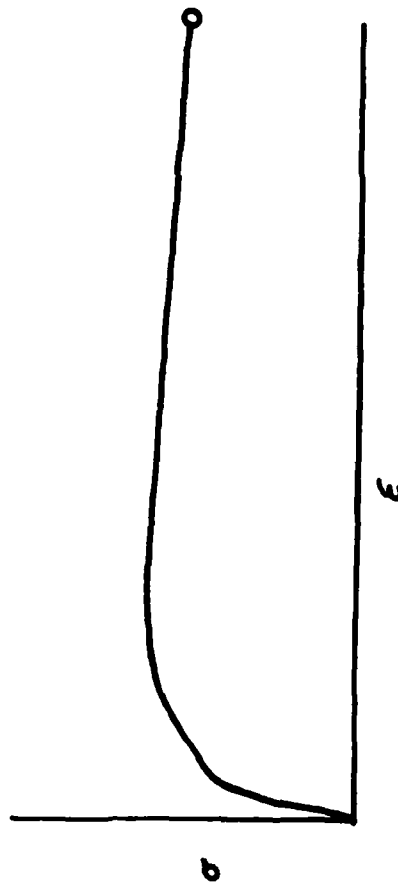
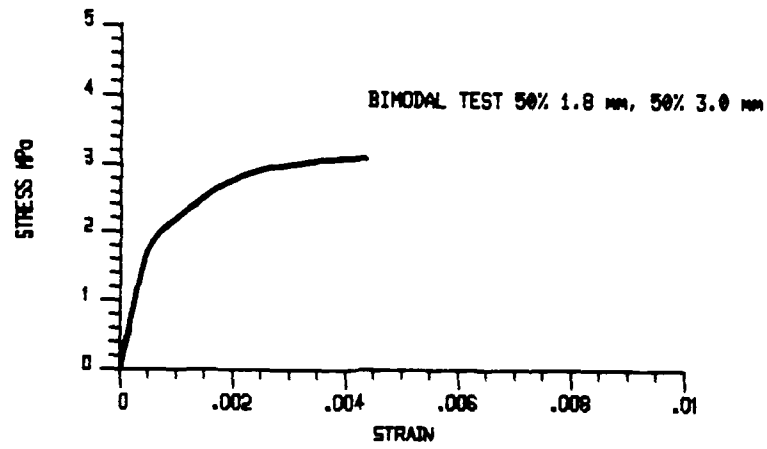
Ready

COMPRESSION TEST JL-4



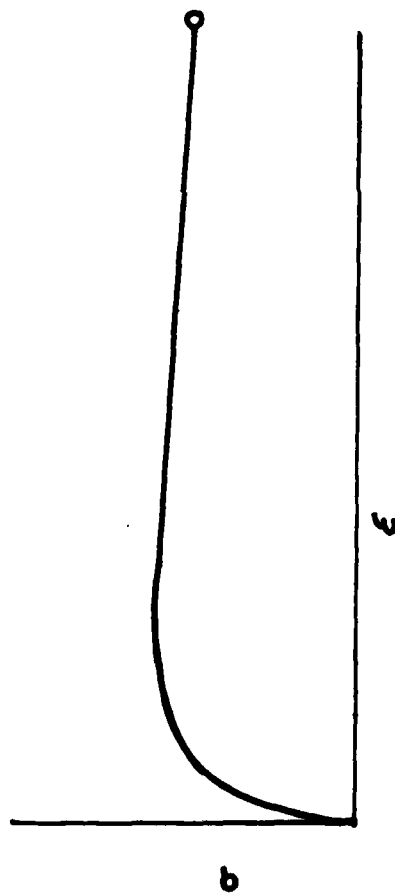
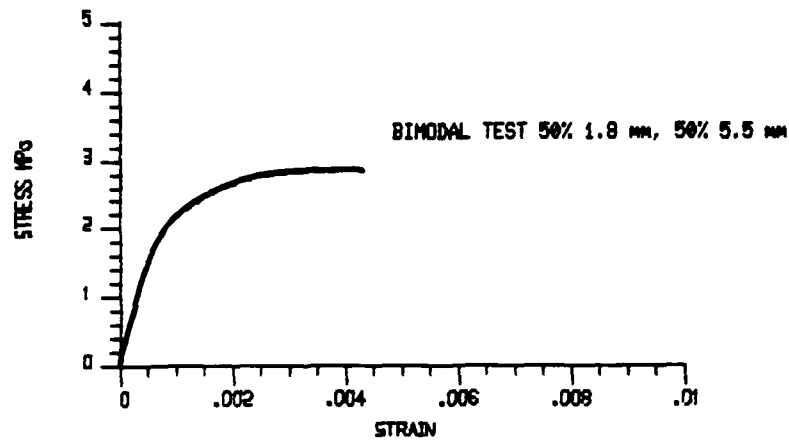
Ready

COMPRESSION TEST JL-5



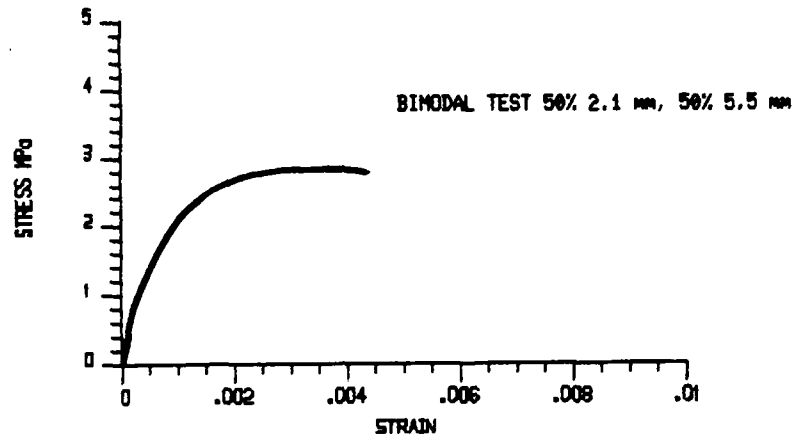
Ready

COMPRESSION TEST JL-6



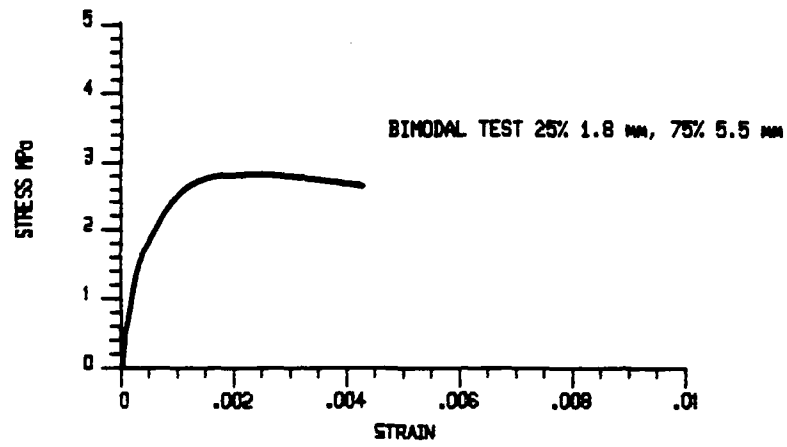
Ready

COMPRESSION TEST JL-7



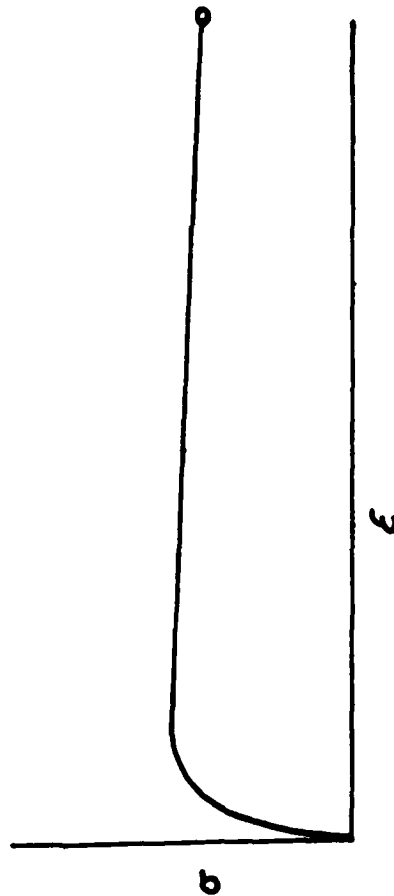
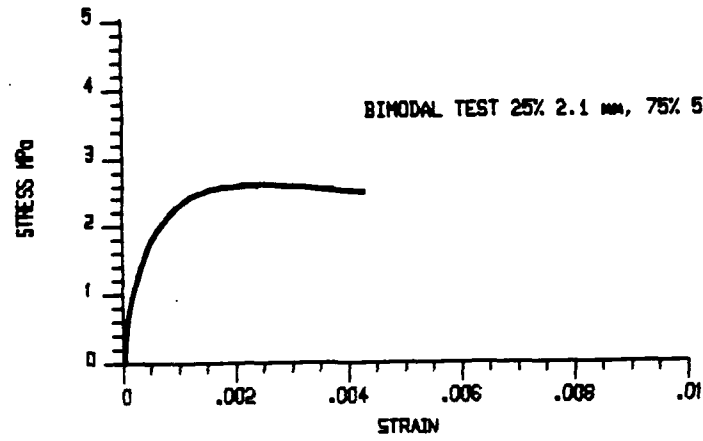
Ready

COMPRESSION TEST JL-8



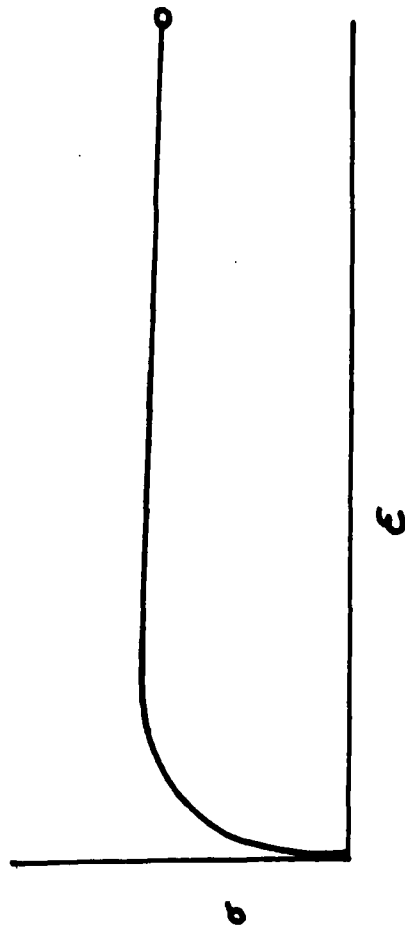
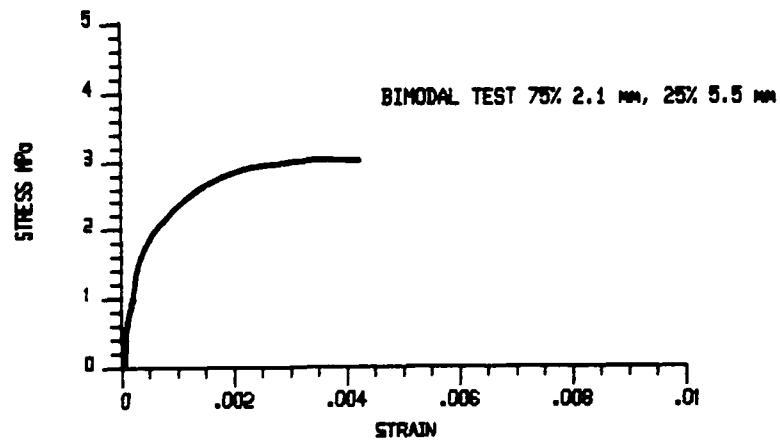
Ready

COMPRESSION TEST JL-9



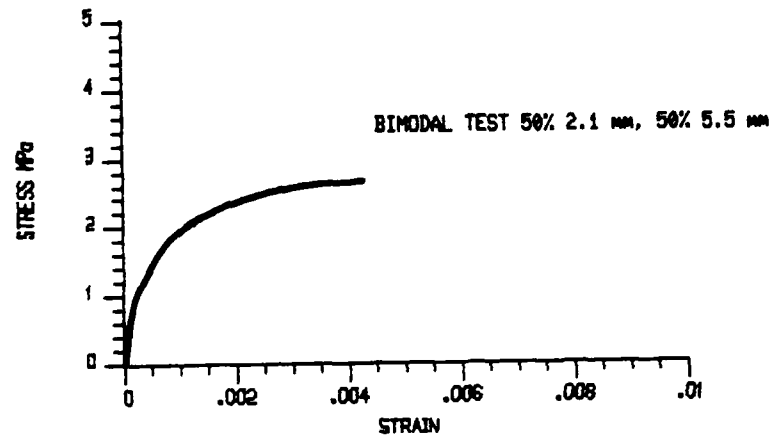
Ready

COMPRESSION TEST JL-10



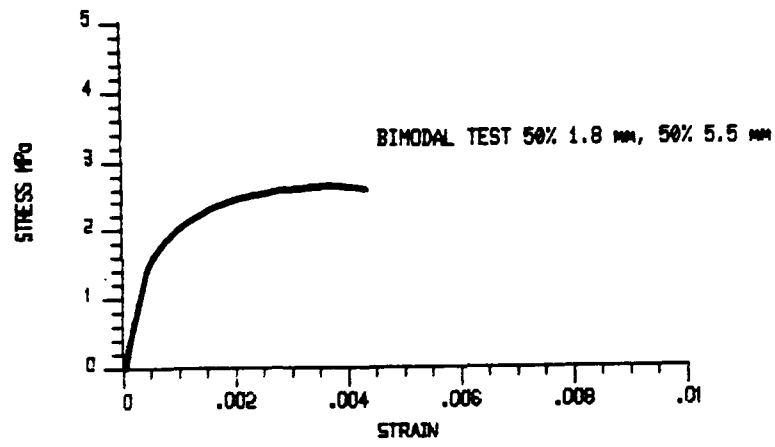
Ready

COMPRESSION TEST JL-12



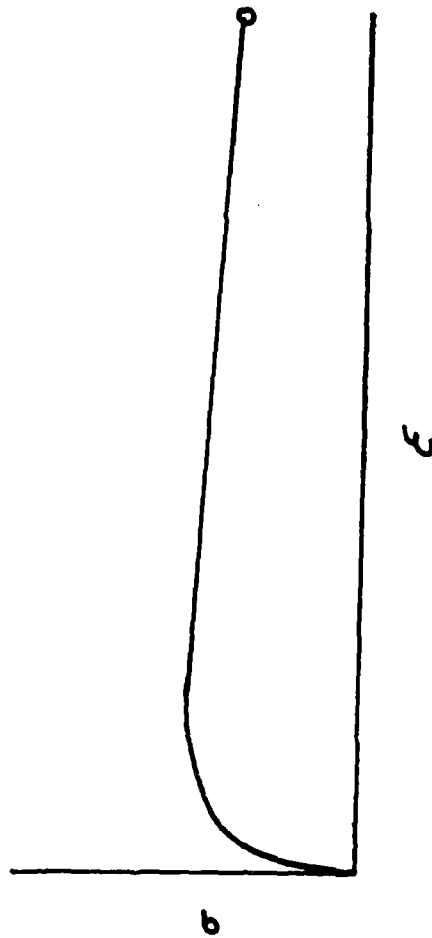
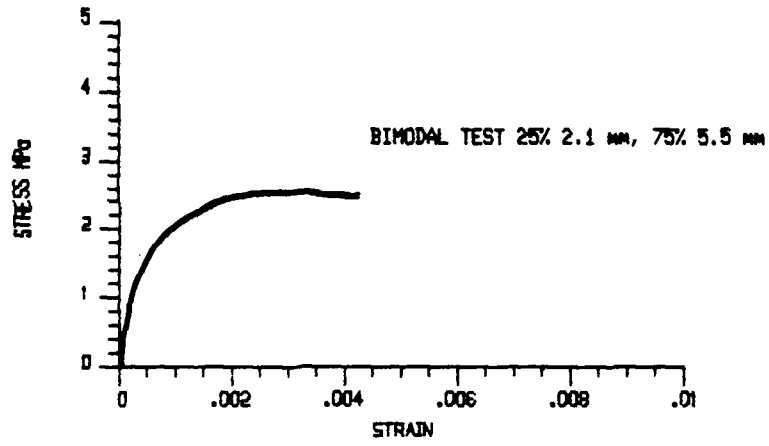
Ready

COMPRESSION TEST JL-13



Ready

COMPRESSION TEST JL-14



AD-A162 361

THE EFFECT OF A BIMODAL GRAIN SIZE DISTRIBUTION ON THE
COMPRESSIVE STRENGTH OF POLYCRYSTALLINE ICE(U) ARMY
MILITARY PERSONNEL CENTER ALEXANDRIA VA J L LAUGHLIN

2/2

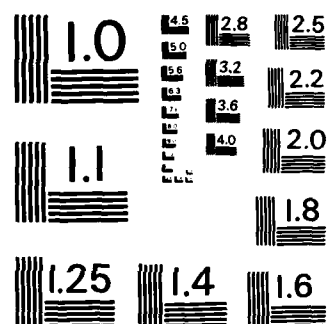
UNCLASSIFIED

DEC 85

F/G 8/12

NL

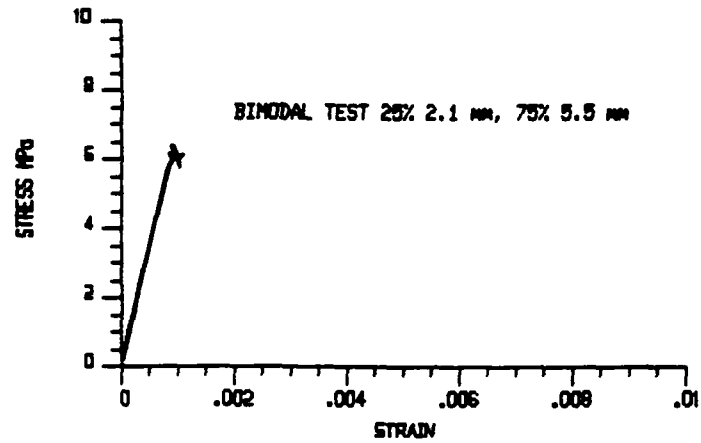




MICROCOPY RESOLUTION TEST CHART
NATIONAL BUREAU OF STANDARDS-1963-A

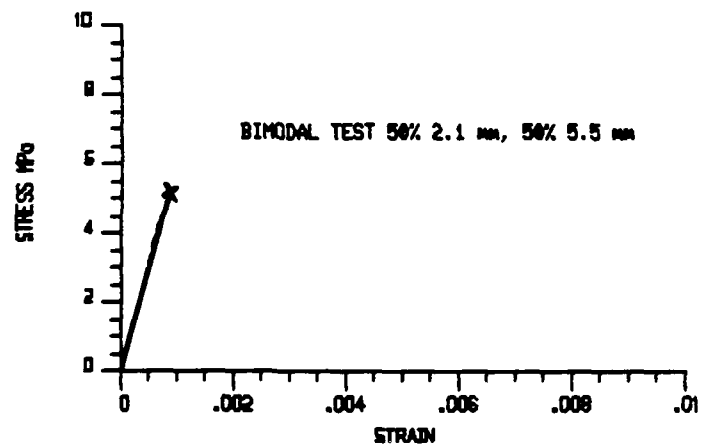
Ready

COMPRESSION TEST JL-15



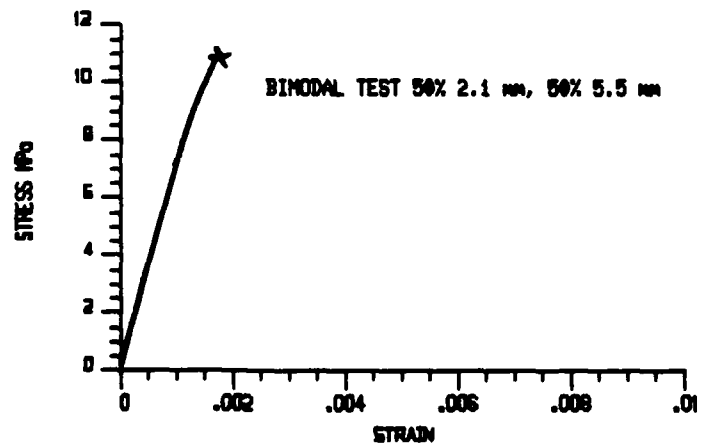
Ready

COMPRESSION TEST JL-16



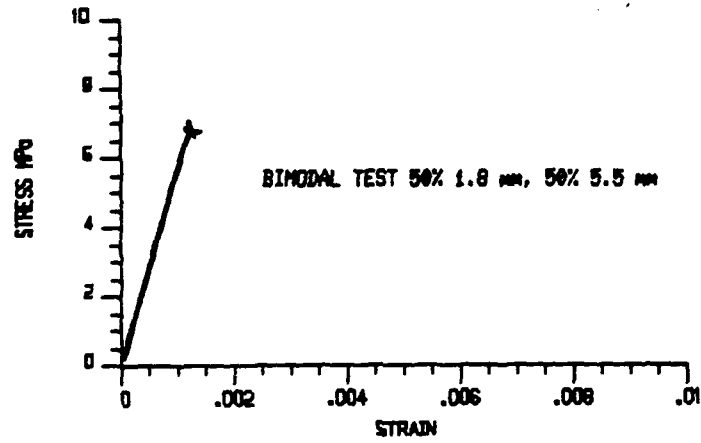
Ready

COMPRESSION TEST JL-18



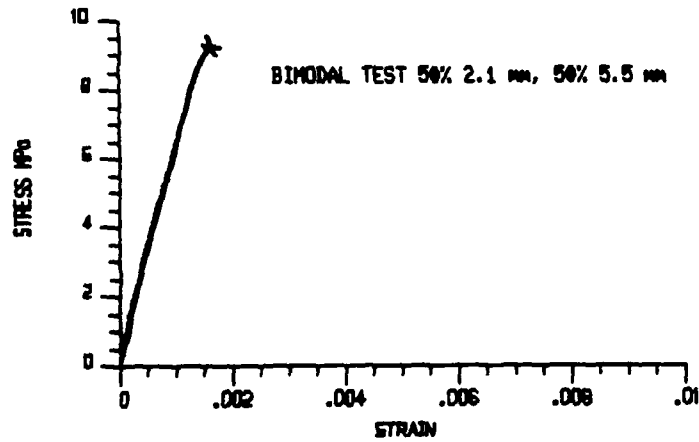
Ready

COMPRESSION TEST JL-19



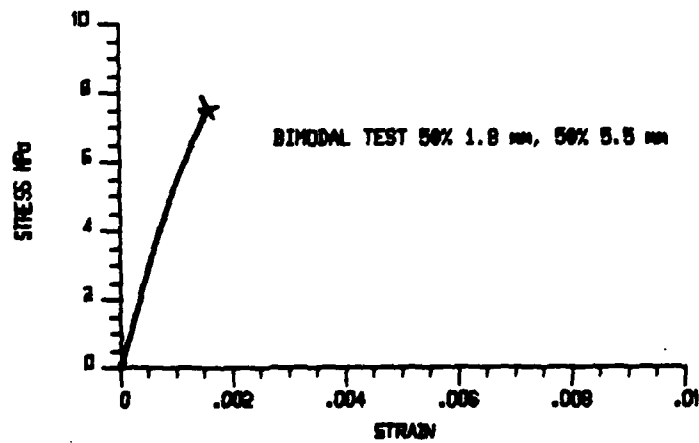
Ready

COMPRESSION TEST JL-20



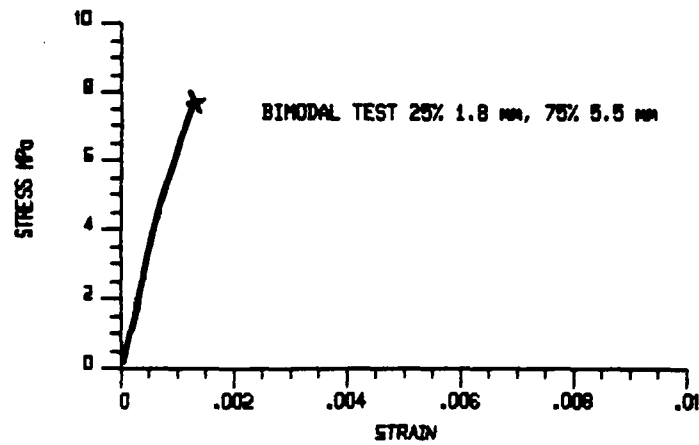
Ready

COMPRESSION TEST JL-21



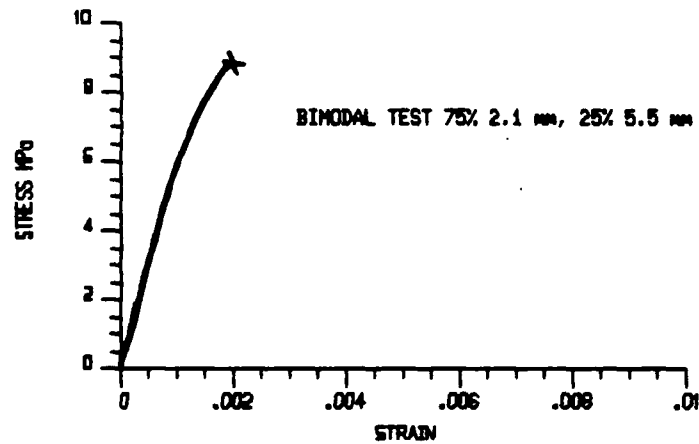
Ready

COMPRESSION TEST JL-26L



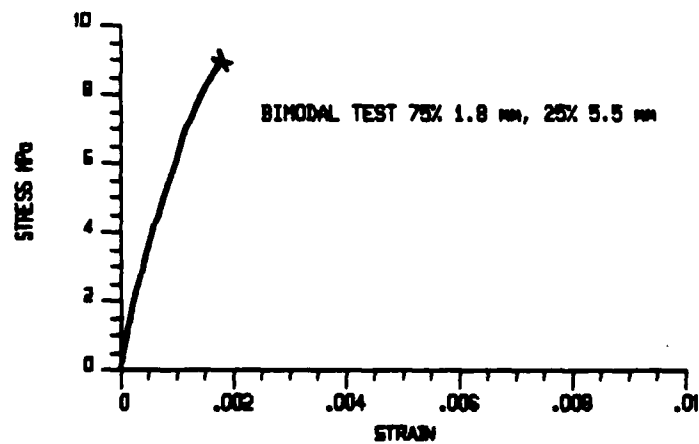
Ready

COMPRESSION TEST JL-26L



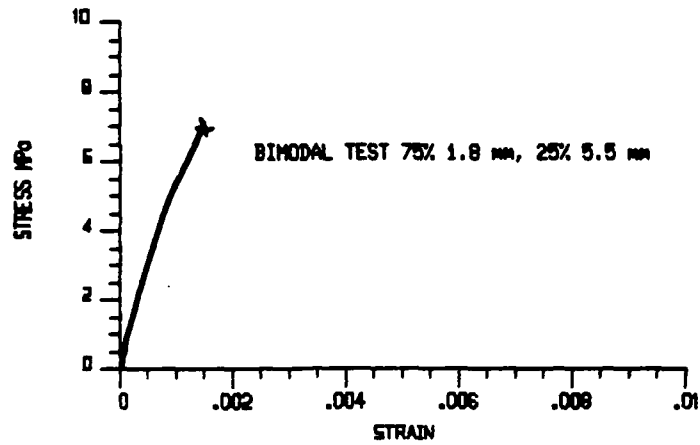
Ready

COMPRESSION TEST JL-27L



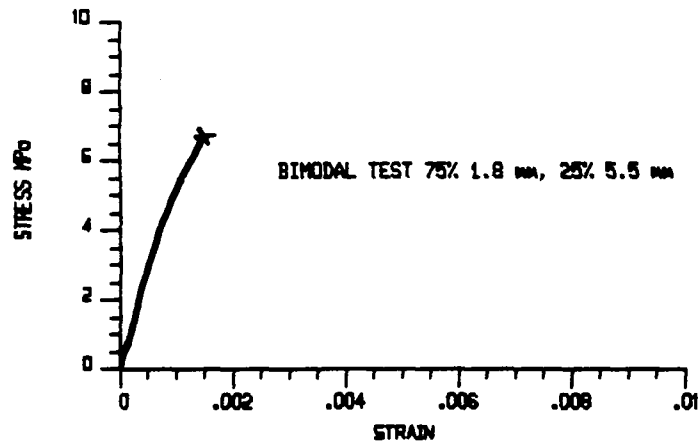
Ready

COMPRESSION TEST JL-28L



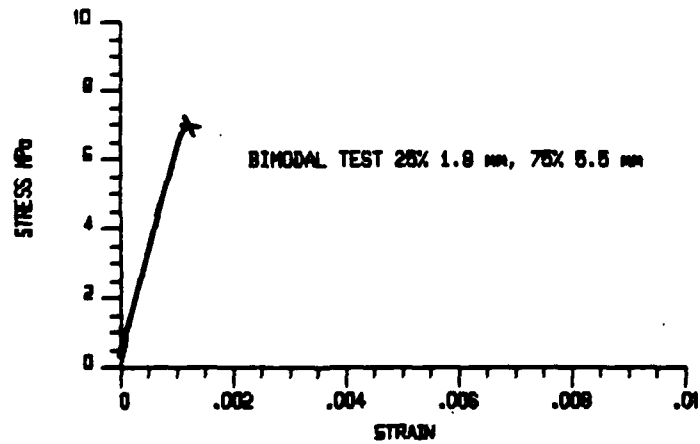
Ready

COMPRESSION TEST JL-28L



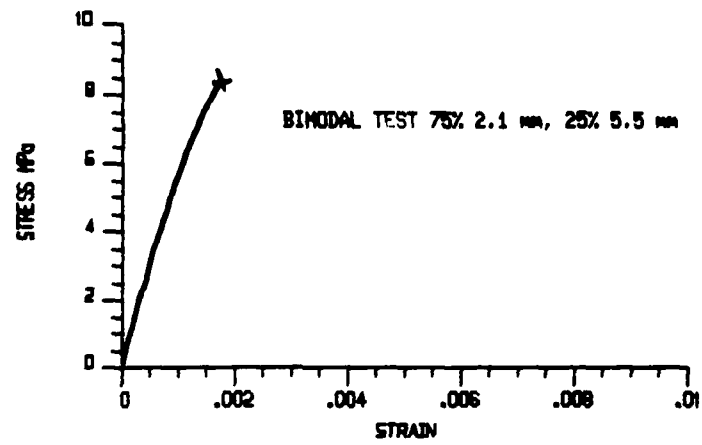
Ready

COMPRESSION TEST JL-42L



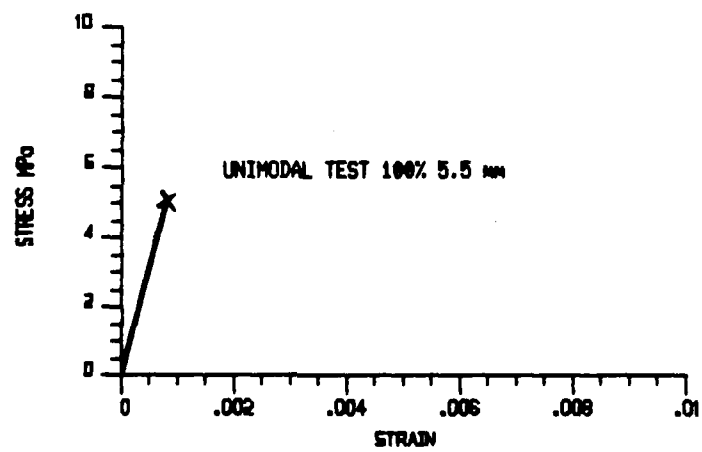
Ready

COMPRESSION TEST JL-42L



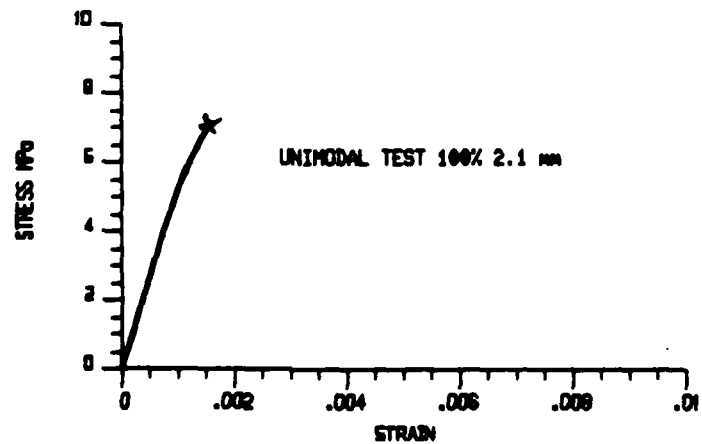
Ready

COMPRESSION TEST JLL-10



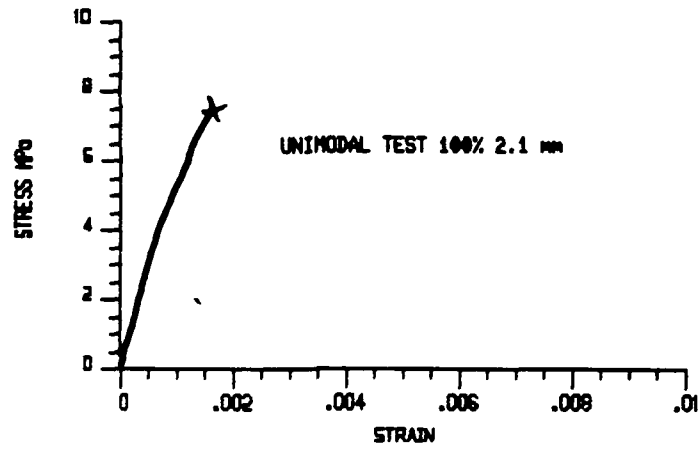
Ready

COMPRESSION TEST JLL-11



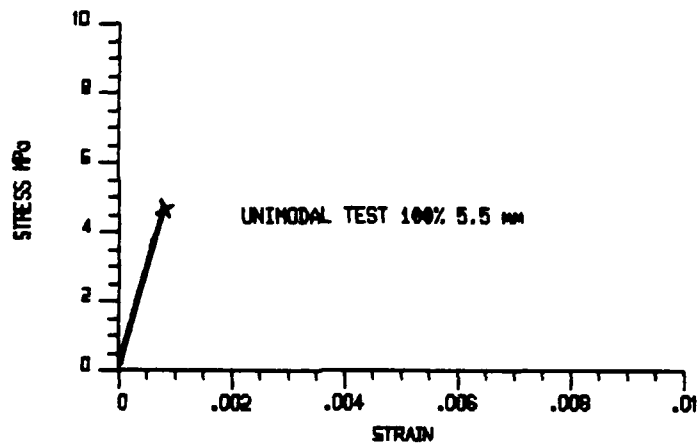
Ready

COMPRESSION TEST JLL-18



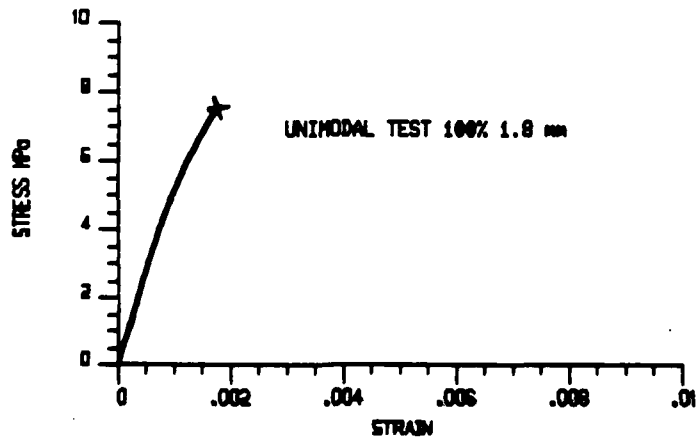
Ready

COMPRESSION TEST JLL-19



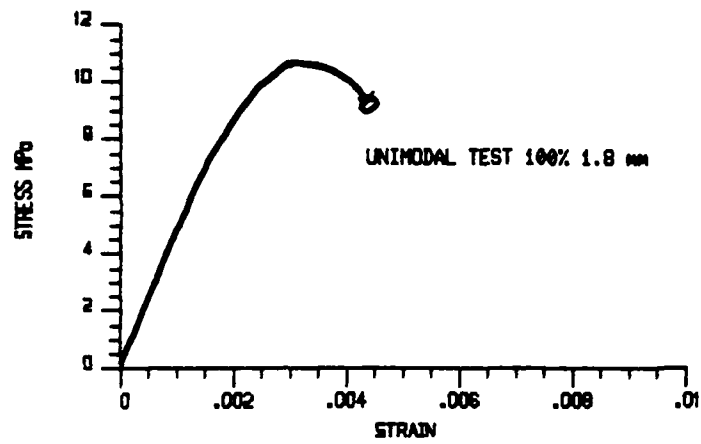
Ready

COMPRESSION TEST B-1



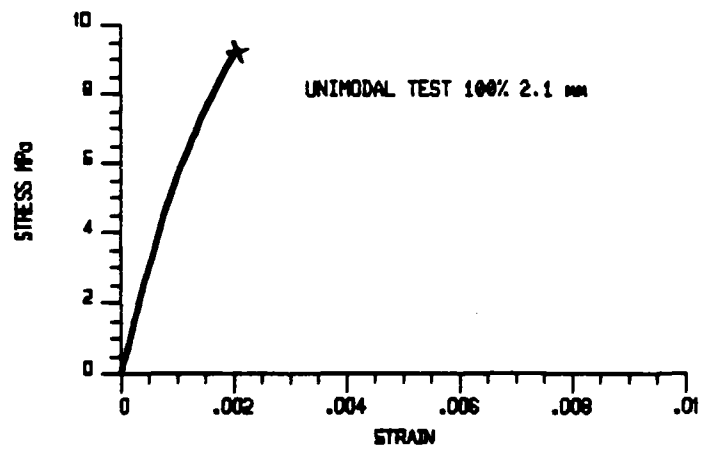
Ready

COMPRESSION TEST 8-2



Ready

COMPRESSION TEST 8-3



APPENDIX C

Appendix C contains the results from testing at 10^{-1}s^{-1} under stroke control. Table C-1 depicts the experimental results and Figure C-1 provides a graph of the strength versus the grain size. The tests show great scatter, as would be expected at this high strain rate. There appears to be no obvious correlation between grain size and strength from this data. This is the same conclusion drawn by Jones and Chew (1983) as a result of their testing under similar control conditions conducted at a strain rate of $5 \times 10^{-4} \text{s}^{-1}$.

Table C-1 Stroke Control Tests at Strain Rate of 10^{-1}s^{-1} (-10°C)

#	Sample	Grain size	Strength (MPa)
	L-8	$2.2 \pm .2 \text{ mm}$	7.93
	L-14	$3.0 \pm .3 \text{ mm}$	3.84
	L-12	$3.5 \pm .3 \text{ mm}$	4.17
	L-16	$3.5 \pm .3 \text{ mm}$	3.95
	L-9	$3.8 \pm .4 \text{ mm}$	7.13
	L-13	$3.8 \pm .4 \text{ mm}$	3.18
	L-5	$4.3 \pm .3 \text{ mm}$	3.51
	L-17	$6.4 \pm .4 \text{ mm}$	3.84
	L-20	$6.4 \pm .4 \text{ mm}$	3.95
	L-6	$7.3 \pm .3 \text{ mm}$	3.73
	L-21	$7.3 \pm .3 \text{ mm}$	3.62

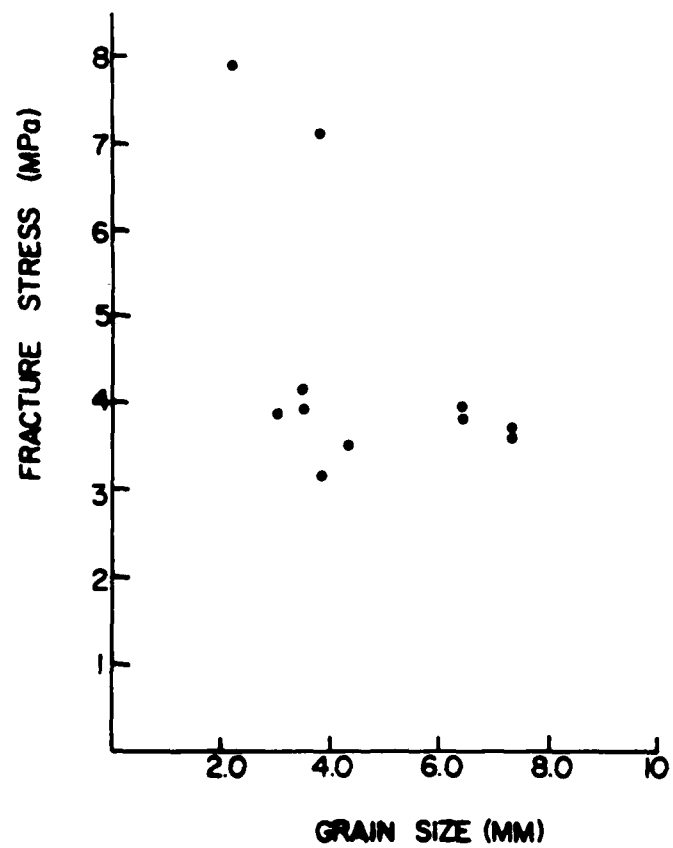


FIGURE C-1 Fracture Stress vs. Grain Size for a Strain Rate of $10^{-1} s^{-1}$,
-10°C Under Stroke Control

END

FILMED

1-86

DTIC